Constraining N20 emissions since 1940 using firn air isotope measurements in both hemispheres

Markella Prokopiou, Patricia Martinerie, Célia Sapart, Emmanuel Witrant, Guillaume Monteil, Kentaro Ishijima, Sophie Bernard, Jan Kaiser, Ingeborg Levin, T. Sowers, et al.

Atmos. Chem. Phys. Discuss., doi:10.5194/acp-2016-487, 2016
Manuscript under review for journal Atmos. Chem. Phys.
Published: 21 June 2016

Atmospheric Chemistry and Physics Discussions

Constraining N_2O emissions since 1940 using firn air isotope measurements in both hemispheres

M. Prokopiou[1], P. Martinerie[2], C. J. Sapart[1,3], E. Witrant[4], G. A. Monteil[1,5], K. Ishijima[6], S. Bernard[2], J. Kaiser[7], I. Levin[8], T. Sowers[9], T. Blunier[10], D. Etheridge[11], E. Dlugokencky[12], R. S. W. van de Wal[1], T. Röckmann[1]

[1] Institute for Marine and Atmospheric research Utrecht, Utrecht, The Netherlands

[2] University of Grenoble Alpes/CNRS, LGGE, F-38000 Grenoble, France

[3] Laboratoire de Glaciologie, ULB, Brussels, Belgium

[4]University of Grenoble Alpes/CNRS, GIPSA-Lab, F-38000 Grenoble, France

[5] Department of Physical Geography and Ecosystem Science, Lund University, Lund, Sweden

[6] National Institute of Polar Research, Tokyo, Japan

[7] Centre for Ocean and Atmospheric Sciences, School of Environmental Sciences, University of East Anglia, Norwich, United Kingdom

[8] Institute of Environmental Physics, Heidelberg University, Germany

[9] Earth and Environmental Systems Institute, Pennsylvania, USA

[10] Centre for Ice and Climate, Niels Bohr Institute, Copenhagen, Denmark

[11] CSIRO Marine and Atmospheric Research, Victoria, Australia

[12] NOAA Earth System Research Laboratory, Boulder, Colorado, USA

Abstract

N_2O is currently the 3rd most important anthropogenic greenhouse gas in terms of radiative forcing and its atmospheric mole fraction is rising steadily. To quantify the growth rate and its causes, we performed a multi-site reconstruction of the atmospheric N_2O mole fraction and isotopic composition using firn air data collected from Greenland and Antarctica in combination with a firn diffusion and densification model. The multi-site reconstruction showed that while the global mean N_2O mole fraction increased from (290±1) nmol mol^{-1} in 1940 to (322±1) nmol mol^{-1} in 2008 the isotopic delta [values] of atmospheric N_2O decreased by (−2.2±0.2) ‰ for $\delta^{15}N^{av}$, (−1.0±0.3) ‰ for $\delta^{18}O$, (−1.3±0.6) ‰ for $\delta^{15}N^{\alpha}$, and (−2.8±0.6) ‰ for $\delta^{15}N^{\beta}$ over the same period. The detailed temporal evolution of the mole fraction and

Atmos. Chem. Phys. Discuss., doi:10.5194/acp-2016-487, 2016
Manuscript under review for journal Atmos. Chem. Phys.
Published: 21 June 2016

Atmospheric Chemistry and Physics Discussions

isotopic composition derived from the firn air model was then used in a two-box atmospheric model (comprising a stratospheric and a tropospheric box) to infer changes in the isotopic source signature over time. The precise value of the source strength depends on the choice of the N_2O lifetime, which we choose to be 123^{+29}_{-19} a. Adopting this lifetime results in total average source isotopic signatures of (−7.6±0.8) ‰ (vs. Air-N_2) for $\delta^{15}N^{av}$, (32.2±0.2) ‰ (vs. VSMOW) for $\delta^{18}O$, (−3.0±1.9) ‰ (vs. Air-N_2) for $\delta^{15}N^{\alpha}$, and (−11.7±2.3) ‰ (vs. Air-N_2) for $\delta^{15}N^{\beta}$ over the investigated period. $\delta^{15}N^{av}$ and $\delta^{15}N^{\beta}$ show some temporal variability while the other source isotopic signatures remain unchanged. The ^{15}N site-preference (= $\delta^{15}N^{\alpha} - \delta^{15}N^{\beta}$) can be used to reveal further information on the source emission origins. Based on the changes in the isotopes we conclude that the main contribution to N_2O changes in the atmosphere since 1940 is from soils, with agricultural soils being the principal anthropogenic component which is in line with previous studies.

1 Introduction

The rise of nitrous oxide (N_2O) since pre-industrial times contributes significantly to radiative forcing (Forster et al., 2007). Over the past four decades, the N_2O mole fraction has increased by 0.25 % per year, reaching 324 nmol mol^{-1} in 2011 (IPCC, ch.6, 2013). Therefore, the understanding of the biogeochemical cycle of N_2O is important for a reliable assessment of future climate change. In addition, the destruction of N_2O in the stratosphere provides an important source of nitrogen oxides (NO_x), which contribute to stratospheric ozone depletion (Ravishankara et al., 2009).

Natural sources of N_2O are microbial processes in soils and oceans, which produce N_2O during nitrification and denitrification (Bouwman et al., 2013; Loescher et al., 2012; Santoro et al., 2011; Galloway et al., 2004; Pérez et al., 2001; Yung and Miller, 1997; Kim and Craig, 1993). The increase of N_2O since pre-industrial times (hereafter referred to as "anthropogenic" increase) has been attributed largely to increased microbial production, resulting from the increased use of nitrogen fertilizers in agriculture. Industry (especially nylon production) and fossil fuel combustion present a smaller contribution to the anthropogenic source (Davidson, 2009; Kroeze et al., 1999; Mosier et al., 1998). N_2O is primarily destroyed in the stratosphere via UV photolysis (90%) and reactions with excited oxygen atoms (10 %) (Minschwaner et al., 1993), with a minor N_2O fraction removed by surface sinks (Syakila, 2010).

Atmos. Chem. Phys. Discuss., doi:10.5194/acp-2016-487, 2016
Manuscript under review for journal Atmos. Chem. Phys.
Published: 21 June 2016

Atmospheric Chemistry and Physics Discussions

Estimates of the total N_2O source strength from various bottom-up and top-down studies suggest a mean value of roughly 17 Tg a^{-1} N equivalents at present. However, the range in both approaches is large, especially for bottom-up estimates, which range between 8.5 and 27.7 Tg a^{-1} N, whereas top-down estimates range between 15.8 and 18.4 Tg a^{-1} N (Potter et al., 2011 and references therein). Besides the total source strength, the contributions of individual source processes are also poorly constrained. Due to the long steady-state lifetime of N_2O in the atmosphere (123^{+29}_{-19} a; SPARC Lifetimes Report 2013), temporal and spatial gradients are small, making it difficult to resolve localised sources.

Measurements of the isotopic composition of N_2O may help to constrain the atmospheric N_2O budget. The N_2O molecule is linear (NNO) and the two N atoms are chemically distinguishable; thus they tend to attain different isotopic compositions. Beyond oxygen ($\delta^{18}O$, $\delta^{17}O$) and average $\delta^{15}N^{av}$ ("bulk") signatures, N_2O also displays site specific ^{15}N isotopic information. Site preference ($\delta^{15}N^{sp}$) is defined as the difference in $\delta^{15}N$ between the central (2, μ or α) and terminal position (1, τ or β) of N atoms in N_2O (Kaiser, 2002; Brenninkmeijer and Röckmann, 2000; Yoshida and Toyoda, 1999), i.e. $\delta^{15}N^{sp} = \delta^{15}N^{\alpha} - \delta^{15}N^{\beta}$. For consistency with many recent publications in the field, we here adopt the nomenclature from Yoshida and Toyoda (1999), α and β, for the two positions.

The different sources and sinks of N_2O are associated with characteristic fractionation processes leading to different isotope ratios. For example, microbial sources emit N_2O that is depleted in ^{15}N and ^{18}O relative to the tropospheric background. N_2O that returns from the stratosphere after partial photochemical removal is enriched in both heavy isotopes (Yoshida and Toyoda, 2000; Yung and Miller, 1997; Kim & Craig, 1993). Stratospheric N_2O also has a high ^{15}N site-preference compared to tropospheric N_2O. The observed enrichment is caused by kinetic isotope fractionation in the stratospheric sink reactions (Kaiser et al., 2006; 2002; Park et al., 2004; Röckmann et al., 2001; Yoshida and Toyoda, 2000).

The multi-isotope signature of N_2O adds useful constraints on its budget. In particular, when the isotopic composition of tropospheric N_2O is combined with the fractionation during its removal in the stratosphere, the isotopic composition of the global average source can be determined (Ishijima et al., 2007; Bernard et al., 2006; Röckmann et al., 2003; Kim and Craig, 1993).

The temporal variations of the N_2O isotopic composition are difficult to quantify on a short timescale because of its long residence time in the atmosphere. Longer time scales can be

Atmos. Chem. Phys. Discuss., doi:10.5194/acp-2016-487, 2016
Manuscript under review for journal Atmos. Chem. Phys.
Published: 21 June 2016

92 reconstructed by using air trapped in Arctic and Antarctic firn and ice which provides a
93 natural archive of past atmospheric composition. The firn phase is the intermediate stage
94 between snow and glacial ice, which constitutes the upper 40-120 m of the accumulation zone
95 of ice sheets. Within the firn, air exchanges relatively freely in the upper layers and with the
96 overlying atmosphere (convective zone). With increasing depth the air pores shrink in size
97 due to firn compaction, and air mixes primarily via slow diffusion in the diffusive zone. At
98 densities larger than ≈815 kg m^{-3}, air is permanently trapped in closed bubbles in the ice and
99 totally isolated from the atmosphere. The precise age range of air that can be retrieved from
100 polar firn between the surface and bubble close-off depends on site specific characteristics
101 like temperature, accumulation rate and porosity and typically ranges from several decades to
102 120 years.

103 For N_2O, a number of studies have reported isotope measurements from different Arctic and
104 Antarctic firn drilling sites showing a steady decrease of the heavy isotope content of N_2O
105 over the past decades (Park et al., 2012; Ishijima et al., 2007; Bernard et al., 2006; Röckmann
106 et al., 2003; Sowers et al., 2002). A more recent study by Park et al. (2012) attempted to
107 reconstruct the long-term trends in N_2O isotopic compositions and its seasonal cycles to
108 further distinguish between the influence of the stratospheric sink and the oceanic source at
109 Cape Grim, Tasmania, demonstrating that isotope measurements can help in the attribution
110 and quantification of surface sources in general.

111 Taking into account the long atmospheric lifetime of N_2O and the fact that both hemispheres
112 are well mixed on annual timescales, it is reasonable to assume that the results from these
113 studies are representative for the global scale. However care needs to be taken because small
114 differences in the diffusivity profiles of the firn column lead to large effect on the isotope
115 signature (Buizert et al. 2012). Interestingly, for atmospheric methane (CH_4), another
116 important greenhouse gas, a recent multi-site analysis on the carbon isotopic composition of
117 showed large differences among reconstructions from different sites (Sapart et al., 2013). In
118 particular, firn fractionation effects related to diffusion and gravitational separation and their
119 implementation in models (Buizert et al., 2012) have large effects on the reconstructed
120 signals. Small differences in the diffusivity profiles of the firn column lead to large effects on
121 the isotope signatures. Therefore, more robust results may be obtained by combining isotope
122 information from a number of different sites in a multi-site reconstruction, including a critical
123 evaluation of diffusivity profiles.

Atmos. Chem. Phys. Discuss., doi:10.5194/acp-2016-487, 2016
Manuscript under review for journal Atmos. Chem. Phys.
Published: 21 June 2016

Atmospheric Chemistry and Physics Discussions

Here we combine new N_2O isotope measurements from the NEEM site in Greenland with previously published firn air N_2O isotope records from 4 different sites from Greenland and Antarctica to reconstruct records of the N_2O isotopic composition over the last 70 years. We use the multi-gas firn transport model established by the Laboratoire de Glaciologie et Géophysique de l'Environnement and Grenoble Image Parole Signal Automatique (LGGE-GIPSA) to obtain an atmospheric scenario that is constrained by and consistent with all individual sites (Allin et al., 2015; Witrant et al., 2012; Wang et al., 2012; Rommelaere et al., 1997). We then use an isotope mass balance model to infer the changes in the isotopic signature of the N_2O source over time to investigate possible changes in the source mix.

2 Materials and Methods

2.1 Firn air Sampling

New firn air samples added in this study to the total dataset were collected in 2008 and 2009 during the firn campaign (Buizert et al., 2011) as part of the North Eemian Ice Drilling programme (NEEM) in Greenland (77.45º N 51.06º W). These data are combined with existing firn air data from four other sites. Information on the locations is provided in Table 1. The firn air collection procedure is described in detail by Schwander et al. (1993). Here a brief description is presented. Essentially a borehole is drilled in the firn to a certain depth and then the firn air sampling device is inserted into the borehole. The device consists of a bladder, a purge line and a sample line. When the sampling device reaches the desired depth the bladder is inflated to seal the firn hole and isolate the air below the bladder from the overlying atmosphere, and air is pumped out from the pore space below the bladder. Continuous online CO_2 concentration measurements are performed to verify that no contamination with contemporary air occurs during the extraction procedure. After the contaminating air has been pumped away, firn air is collected in stainless steel, glass or aluminium containers.

2.2 N_2O isotope analysis

The firn air samples from NEEM are analyzed for N_2O isotopocules at the Institute for Marine and Atmospheric research Utrecht (IMAU). The N_2O mole fraction and isotopic composition are measured using continuous flow isotope ratio mass spectrometry (IRMS). The method is described in detail by Röckmann et al. (2003b). Here only a brief summary is

Atmos. Chem. Phys. Discuss., doi:10.5194/acp-2016-487, 2016
Manuscript under review for journal Atmos. Chem. Phys.
Published: 21 June 2016

Atmospheric Chemistry and Physics Discussions

given. The firn air sample (333 mL) is introduced into the analytical system at a flow rate of 50 mL/min for 400 s. After CO_2 is removed chemically over Ascarite, N_2O and other condensable substances are cryogenically preconcentrated. After cryo-focusing the sample the remaining traces of CO_2 and other contaminants are removed on a capillary GC column (PoraPlot Q, 0.32 mm i.d., 25 m). The column is separated into a pre-column and an analytical column. This set-up eliminates interferences from other atmospheric compounds that have much longer retention times. Finally the sample is transferred to the IRMS via an open split interface. For the new NEEM samples reported here, each firn air sample has been measured five times. Before and after each sample we measured five aliquots of air from a reference cylinder with known isotopic composition and mole fraction for calibration purposes.

$\delta^{15}N$ values are reported with respect to Air-N_2 while $\delta^{18}O$ refers to Vienna Standard Mean Ocean Water (VSMOW). As laboratory reference gas we used an atmospheric air sample with an N_2O mole fraction of 318 nmol mol^{-1} and δ values of (6.4±0.2) ‰ for $\delta^{15}N^{av}$ vs. Air-N_2, (44.9±0.4) ‰ for $\delta^{18}O$ vs. VSMOW. The intramolecular $\delta^{15}N^{av}$ values of the air standard are $\delta^{15}N^{\alpha}$ = (15.4±1.2) ‰ and $\delta^{15}N^{\beta}$ = (–2.7±1.2) ‰. The calibration of the intramolecular distribution follows Toyoda and Yoshida (1999). Typically the 1σ standard deviation of replicate sample measurements are 0.1 ‰ for $\delta^{15}N$, 0.2 ‰ for $\delta^{18}O$ and 0.3 ‰ for $\delta^{15}N^{\alpha}$ and $\delta^{15}N^{\beta}$.

2.3 Modelling trace gas transport in firn

In firn air, the interstitial gas is not yet isolated in closed-off bubbles, so diffusion processes and gravitational separation alter mole fractions and isotope ratios over time. Thus, firn air measurements cannot be used directly to derive the atmospheric history of trace gas signatures. Over time, atmospheric compositional changes are propagated downwards into the firn based on the diffusivity of the atmospheric constituent in question. Firn air diffusion models take these effects into account and thereby allow reconstruction of changes in the atmospheric composition from the firn profile.

In this study we use the LGGE-GIPSA firn air transport model to reconstruct the temporal evolution of N_2O mole fraction and isotopic composition from the measured firn profiles (Allis et al., 2015; Witrant et al., 2012; Wang et al., 2012; Rommelaere et al., 1997).

Atmos. Chem. Phys. Discuss., doi:10.5194/acp-2016-487, 2016
Manuscript under review for journal Atmos. Chem. Phys.
Published: 21 June 2016

Atmospheric Chemistry and Physics Discussions

In the "forward version" of LGGE-GIPSA, a physical transport model uses a historic evolution of atmospheric N_2O mole fractions to calculate the vertical profiles of mole fractions in firn. For the isotopocules, further simulations are performed separately to calculate their respective vertical profiles. Important parameters needed to constrain the model are the site temperature, accumulation rate, depth of the convective layer and close-off depth, together with profiles of firn density and effective diffusivity. The latter parameter is determined as a function of depth for each firn-drilling site by modelling the mole fractions in firn for trace gases with well known atmospheric histories (Buizert et al., 2012; Witrant et al., 2012; Rommelaere et al., 1997; Trudinger et al., 1997). A multi-gas constrained inverse method (Witrant et al., 2012) is used to calculate the effective diffusivity of each site for each specific gas. It is noteworthy that diffusivity is not constrained equally well at all sites because different sets of constraints (e.g. number of available reference gases) are used at different sites and because of different depth resolutions.

A Green-function approach as presented by Rommelaere et al. (1997), with an extension for isotopic ratios and revised to take into account the sparsity of the measurements (Witrant and Martinerie, 2013; Martinerie et al., 2012; Wang et al., 2011) is used to assign a mean age and age distribution to a certain depth.

Due to the long N_2O residence time in the atmosphere, the global variability of the isotopic composition of N_2O is very small and no significant variations between individual background locations have been detected so far (Kaiser et al., 2003). In particular, the isotope ratio difference between northern and southern hemisphere tropospheric air is expected to be only –0.06 ‰ (based on an interhemispheric mole fraction gradient of 1.2 nmol mol^{-1} [Hirsch et al. 2006] and isotope ratio difference of –15 ‰ between average source and average tropospheric isotope delta). These differences are within the uncertainties of the firn air measurements used here and therefore the data from the northern and southern hemisphere are combined into a single dataset without including an interhemispheric gradient.

With the multi-site reconstruction method, we used the measurements from six firn air drillings at five sites (NEEM-09, NEEM-EU-08, NGRIP-01, BKN-03, DC-99, DML-98) to constrain our model and determine a set of atmospheric reconstructions that fits all sites. Data from Ishijima et al. (2007) and Sowers et al. (2002) [NGRIP-01 and SP-01, SP-95 respectively] were not included in our multi-site reconstruction because no data for $\delta^{15}N^{\alpha}$ and

Atmos. Chem. Phys. Discuss., doi:10.5194/acp-2016-487, 2016
Manuscript under review for journal Atmos. Chem. Phys.
Published: 21 June 2016

$\delta^{15}N^{\beta}$ were published for those sites. These datasets were used for independent validation of $\delta^{15}N^{av}$ and $\delta^{18}O$.

To quantify the isotope fractionation due to diffusion and gravitational settling within the firn, a forward firn transport model simulation was carried out with a realistic N_2O mole fraction scenario (based on the Law Dome record, MacFarling Meure et al., 2001), but with a constant isotopic N_2O history. This allows determining the role of transport isotope fractionation occurring in the firn, in the absence of isotopic changes in the atmosphere. The results are used to subtract the firn fractionation effects from the measured signals, which can then be used to assess the atmospheric history. Compared to the signal, the effect of firn fractionation is minor for $\delta^{15}N$, but important for $\delta^{18}O$ especially at the lower accumulation rates in the Southern Hemisphere (see Appendix A).

The deepest firn data from each site provide constraints furthest back in time and the oldest air samples that are included in the inversion are from the DML-98 and DC-99, which extend the reconstruction of atmospheric N_2O back to the early 20th century (Röckmann et al., 2003). At the same, the correction for isotopic fractionation in firn is most uncertain for the deepest samples, where strong differences between individual firn air models have been reported (Buizert et al., 2012).

2.4 Scaling of different data sets

At present, no international reference materials for the isotopic composition of N_2O exist. Kaiser et al. (2003) and Toyoda et al. (1999) linked the isotopic composition of N_2O in tropospheric air to the international isotopes scales for nitrogen isotopes (Air-N_2) and oxygen isotopes (either VSMOW or Air-O_2). Our measurements are linked to a standard gas cylinder of tropospheric air with known N_2O mole fraction and isotopic composition based on the scale of Kaiser et al. (2003) for $\delta^{15}N^{av}$ and $\delta^{18}O$ values and Yoshida and Toyoda (1999) for position dependent ^{15}N values. However, the reference air cylinder used for the calibration was exhausted and had to be replaced three times over the years in which the different measurement that we combine in this study were performed. Although the cylinders were carefully compared, the long-time consistency of the isotope scale could not be guaranteed because long-time isotope standards are not available. In fact, analysis of the data from the convective zone for the different sites, show small but significant differences from the temporal trends that are well established from previously published data from the German

Atmos. Chem. Phys. Discuss., doi:10.5194/acp-2016-487, 2016
Manuscript under review for journal Atmos. Chem. Phys.
Published: 21 June 2016

Atmospheric Chemistry and Physics Discussions

Antarctic Georg von Neumayer station for 1990 to 2002 (Röckmann and Levin; 2005). The linear trends reported in that paper are (–0.040±0.003) ‰ a^{-1} for $\delta^{15}N^{av}$, (0.014±0.016) ‰ a^{-1} for $\delta^{15}N^{\alpha}$, (–0.064±0.016) ‰ a^{-1} for $\delta^{15}N^{\beta}$ and (–0.021±0.003) ‰ a^{-1} for $\delta^{18}O$. Since they were derived from direct air samples (unaffected by firn fractionation), these trends can be used as a reference to re-scale the different firn air results from different dates. To do so, data from the diffusive zone ($\rho < 815$ kg m^{-3}) for each individual site were scaled to one reference site, DC-99, taking into account the temporal differences in sampling and the model-assigned mean age of the firn air samples (see below). DC-99 was chosen as reference site because it has most measurements in the diffusive zone. Also, the precision of these measurements was high because high volume cylinders were available from which many measurements could be performed and averaged. To test the sensitivity to the choice of reference site, we repeated the re-scaling using NEEM-09 as reference, which generated almost identical results within uncertainty bars (Appendix C).

The average difference between the samples from the diffusive zone at a given site and the interpolated DC-99 results was compared to the expected temporal trend between the sampling date of each station and DC-99, using the temporal trends established by Röckmann and Levin (2005), as shown in the equations below. The effect of this scaling is that the temporal trend in the past decade is effectively forced to follow the atmospheric measurements at Neumayer station (Röckmann and Levin, 2005).

After re-scaling the firn isotopic data we detected some individual data points that clearly deviated from the general trends. These were considered outliers, because they exceeded the 2σ error, and were removed from the dataset. All of these values are site-specific ^{15}N values, specifically, the following, were excluded: NEEM-EU-08 hole depth –4.9 m, –34.72 m, –61.95 m and –74.5 m, and NEEM-09 hole depth 1.0 m, 0.2 m and –69.4 m.

The mole fraction data that can be obtained from the NEEM air isotope measurements were substituted with more precise measurements of N_2O mole fraction by the Commonwealth Scientific and Industrial Research Organisation (CSIRO) the Institute of Environmental Physics, University of Heidelberg (IUP), the Centre of Ice and Climate, University of Copenhagen (CIC) and National Oceanic and Atmospheric Administration (NOAA). In this way we combine all available N_2O mole fraction data.

The mole fraction data were scaled to the most recent international scale, NOAA-2006A from the CSIRO scale or the NOAA-2000 scale. Conversion of the NOAA-2000 data to the

Atmos. Chem. Phys. Discuss., doi:10.5194/acp-2016-487, 2016
Manuscript under review for journal Atmos. Chem. Phys.
Published: 21 June 2016

Atmospheric Chemistry and Physics Discussions

NOAA-2006A scale is done using a conversion factor available by National Oceanic and Atmospheric Administration (NOAA) (http://www.esrl.noaa.gov/gmd/ccl/scales/N2O_scale.html). Converting from the CSIRO to the NOAA-2006A scale, though, requires the reference cylinder details, which were not available. Instead we used a trend scenario, based on the CSIRO atmospheric scale combined with Law Dome data and assuming a constant interhemispheric gradient. This trend scenario was then compared with the data provided on NOAA-2006A scale, and a polynomial fit was generated, which was then used to convert the data to the NOAA-2006A scale. All results presented in the next section are based on the scaling procedure and removal of the outliers as described above (Appendix B).

2.5 Global N_2O (isotope) budget calculations

The tropospheric budget is controlled by N_2O emissions from natural and anthropogenic sources at the surface and by the exchange between troposphere and stratosphere. A simple two-box model is used to quantitatively understand the emissions and the budget changes of N_2O. The model consists of a tropospheric N_2O reservoir (index T) into which N_2O is emitted from natural (E_{nat}) and anthropogenic (E_{anth}) sources. N_2O is then transported to the stratosphere (index S) where part of it is destroyed by photochemical reactions (F_{sink}), and the remainder returns from the stratosphere to the troposphere (TS_{exch}).

The change in the tropospheric N_2O reservoir is given by the following mass balance equations (Allin et al, 2015):

$$n_T \frac{d\chi_T}{dt} = E_{nat} + E_{anth} - F_{exch}(\chi_T - \chi_S) \quad (1)$$

$$n_S \frac{d\chi_S}{dt} = F_{exch}(\chi_T - \chi_S) - L \quad (2)$$

where n is the amount of air and χ_S and χ_T are the mole fractions of N_2O in the stratosphere and troposphere respectively. Annual fluxes between the two reservoirs, F_{exch}, are calculated based on previous estimates (Appenzeller et al., 1996; Holton et al., 1990). The loss due to stratospheric sink is determined by:

$$L = \frac{n_T\chi_T + n_S\chi_S}{\tau} \quad (3)$$

where τ is the atmospheric lifetime of 123^{+29}_{-19} a.

Atmos. Chem. Phys. Discuss., doi:10.5194/acp-2016-487, 2016
Manuscript under review for journal Atmos. Chem. Phys.
Published: 21 June 2016

Atmospheric Chemistry and Physics Discussions

306 The isotopic budgets are calculated by simply multiplying the reservoir sizes with the
307 corresponding δ values of the different flux terms:

308 $$n_T \frac{d\chi_T\delta_T}{dt} = E_{nat}\delta_{nat} + E_{anth}\delta_{anth} + F_{exch}(\chi_S\delta_S - \chi_T\delta_T) \quad (4)$$

309 $$n_S \frac{d\chi_S\delta_S}{dt} = F_{exch}(\chi_T\delta_T - \chi_S\delta_S) - L\delta_L \quad (5)$$

310 Solving equations 4 and 5 and substituting equations 1 and 2 we reach the final isotope
311 equations:

312 $$n_T \frac{d\delta_T}{dt} = \frac{E_{nat}}{\chi_T}(\delta_{nat} - \delta_T) + \frac{E_{anth}}{\chi_T}(\delta_{anth} - \delta_T) + \frac{F_{exch}\chi_S}{\chi_T}(\delta_S - \delta_T) \quad (6)$$

313 $$n_S \frac{d\delta_S}{dt} = \frac{F_{exch}\chi_T}{\chi_S}(\delta_T - \delta_S) - \frac{L}{\chi_S}\varepsilon_L \quad (7)$$

314 where δ_T is either $\delta^{15}N^{av}$, $\delta^{18}O$, $\delta^{15}N^{\alpha}$, $\delta^{15}N^{\beta}$ from the multi-site reconstruction as shown
315 below. δ_{nat} and δ_{anth} is the isotopic composition of the natural and anthropogenic N_2O source,
316 respectively (our target quantity). ε_L is the apparent fractionation factor associated with
317 stratospheric destruction.

318 δ_S is also not known in this case, but can be calculated using the analogue from Röckmann et
319 al. (2003) by employing the observed apparent Rayleigh fractionation in the stratosphere
320 (ε_{app}). Based on this, the relative isotope ratio difference between the stratosphere and the
321 troposphere can be calculated by:

322 $$\delta_S = \left[(\delta_T + 1)\left(\frac{\chi_S}{\chi_T}\right)^{\varepsilon_{app}} - 1\right] \quad (8)$$

323 where ε_{app} represents the stratospheric fractionation constant associated with this removal
324 process. Here, we used the average ε_{app} of all lowermost stratospheric measurements from
325 Kaiser et al. (2006) (Table 3). Note that slightly different fractionations ε_{app} have been used
326 in previous studies by Röckmann (2001) and Park et al. (2012; 2004) and the sensitivity to
327 these differences will be examined below.

328 Furthermore we assume that the N_2O lifetime and ε_{app} remained constant from pre-industrial
329 time to 2008, thus the annual strength removal can be scaled down from its current value at
330 χ_T= 322 nmol mol^{-1} to the pre-industrial level of $\chi_{T,pi}$ =270 nmol mol^{-1} and the relative

Atmos. Chem. Phys. Discuss., doi:10.5194/acp-2016-487, 2016
Manuscript under review for journal Atmos. Chem. Phys.
Published: 21 June 2016

Atmospheric Chemistry and Physics Discussions

enrichment of stratospheric N_2O relative to tropospheric N_2O described by Eq. 8 remains constant over time. The effect of changing the N_2O lifetime is examined below.

Furthermore it is hypothesized that during the pre-industrial period only natural emissions occurred without any anthropogenic input. After the industrialization (≈1750) any increase in the emission budget is considered to be due to anthropogenic input while natural emissions remain constant, allowing separation of E_{nat} and E_{anth}.

Hence, the isotopic signature of the pre-industrial (natural) N_2O source calculated this way also represents the isotopic signature of the natural source at present, and consequently the average isotopic composition of N_2O originating from "anthropogenic" sources (δ_{anth}) can be estimated.

2.6 Uncertainty estimation using random scenarios

The precision of the calculated N_2O emissions (E_{nat}, E_{anth}) depends primarily on the precision of the atmospheric reconstruction of the N_2O mole fraction (χ_T). However, the uncertainty envelope provided by the firn air reconstruction is insufficient to quantify the uncertainty on the atmospheric N_2O reconstruction: the year-to-year variability of N_2O is constrained by the N_2O lifetime in the troposphere, which is very small in comparison to the width of the reconstructions confidence interval. Possible realistic N_2O scenarios are scenarios that are within the confidence intervals provided by the atmospheric reconstructions, and that have realistic year-to-year variability.

Mathematically, this can be represented by an uncertainty variance covariance matrix **B**, where the diagonal elements (variances) are the yearly uncertainties on the atmospheric N_2O mole fractions, and the off-diagonals are the covariances of the uncertainties of different years. The covariance between the uncertainty on the reconstruction in one year *i* and the uncertainty in another year *j* is defined as:

$$cov(i,j)=r_{i,j}\sigma_i\sigma_j \quad (9)$$

$$r_{i,j}=f(|i-j|) \quad (10)$$

The correlation ($r_{i,j}$) is maximum between two consecutive years, and decreases as the time difference increases.

Atmos. Chem. Phys. Discuss., doi:10.5194/acp-2016-487, 2016
Manuscript under review for journal Atmos. Chem. Phys.
Published: 21 June 2016

We generated an ensemble of 50 random realistic N_2O scenarios within the uncertainty envelope of the firn atmospheric N_2O reconstruction constrained by the covariance matrix **B**. For each of these atmospheric N_2O scenarios, we calculated the corresponding N_2O emission time series. The range of emissions from these scenarios then provides a realistic estimate for the uncertainty in N_2O emissions.

We carried out the same analysis for the different N_2O isotopocules: for each isotopocule (δ value), we generated a covariance matrix $\mathbf{B}^{\delta}$, constrained by the uncertainty ranges provided by the atmospheric reconstructions and the correlation coefficients defined in Eq.6 and Eq.7 to generate a set of 50 random scenarios within the uncertainty envelopes. For each of these random scenarios, we calculated the corresponding source signature scenario and the range in the results provides an uncertainty estimate of the isotopic source signatures.

3 Results

3.1 Mean age

The mean age of N_2O in air sampled from different depths in the firn for all datasets that are used in this study is shown in Fig. 1. The strong change in the mean age gradient that is clearly visible in each profile reflects the transition between the diffusive and bubble close-off zones, which occurs at a specific depth and mean age for each site (marked with x on Fig.1). Fig. 1 also shows that for each site the few samples that are collected within the bubble close-off zone provide the constraints for most of the reconstructed record (for instance, at BKN-03, 50 m depth is the beginning of the bubble close-off zone). In addition to the mean age, the width of the age spectrum also increases with depth. Therefore, the temporal resolution of signals that can be reconstructed from the firn air measurements reduces with depth and approaches the one of ice core samples towards the bottom of the bubble close-off zone.

The Greenland sites (NH) have similar meteorological and glaciological conditions (Table 1), thus the differences between the mean age profiles in Fig. 1 are small. The Antarctic sites (SH) show clear differences because the meteorological and glaciological variables differ strongly from site to site. As a result the firn-ice transition is at a different depth for each location (e.g., the firn-ice transition zone for DML-98 is located at about 73.5 m compared to about 99.5 m at DC-99).

Atmos. Chem. Phys. Discuss., doi:10.5194/acp-2016-487, 2016
Manuscript under review for journal Atmos. Chem. Phys.
Published: 21 June 2016

Atmospheric Chemistry and Physics Discussions

3.2 Experimental results and multi-site reconstruction

Mole fraction and isotopic composition of N_2O in firn air are presented versus depth of the firn air sampling in the middle panels of Fig. 2. The mole fraction decreases with depth in qualitative agreement with the known increase of N_2O in the atmosphere over time. In contrast, all isotope deltas slowly increase with depth in the upper firn and show stronger heavy isotope enrichment in the close-off zone, both indicating heavy isotope depletion in atmospheric N_2O with time.

The atmospheric history that has been reconstructed from these firn datasets using the multi-site inversion (using the data from NEEM-09, NEEM-EU-08, NGRIP-01, BKN-03, DC-99, DML-98) as described in section 2.4 is shown in the left panels of Fig. 2. The solid line shows the scenario that leads to the best fit with all firn data in the middle panel, and the dashed lines show the upper and lower range of possible scenarios that would still produce an acceptable fit to the data within the uncertainty bars. Color-coded symbols show data plotted at their respective mean age (as derived from the firn air model). When the best-fit scenario is used as input for the forward firn air model for each individual site, the model produces the vertical profiles that are shown as coloured lines together with the data in the middle panels. For the sites that were included in the multi-site reconstruction, the firn profiles based on the best-fit scenarios generally match the experimental data points well, which is expected after a successful inversion procedure and with consistent data sets. The right panels in Fig. 2 show the differences between these model results and the data. For the data that were used in the multi-site inversion the model-data differences are generally very small, although individual firn drilling sites in some cases show small systematic deviations, in particular in the close-off zone. This means that when inversions would have been performed on individual sites, the optimal reconstructions would be slightly different. The advantage of the multi-site reconstruction is that the reconstructed scenario is constrained by all sites and all sampling depths. Despite the small differences between individual sites, the left panels show that all data fall within the uncertainty bars of the reconstructed scenario of the inversion.

From 1940 to 2008 the total changes of the δ values of atmospheric N_2O are (–2.2±0.2) ‰ for $\delta^{15}N^{av}$, (–1.0±0.3) ‰ for $\delta^{18}O$, (–1.3±0.6) ‰ for $\delta^{15}N^{\alpha}$ and (–2.8±0.6) ‰ for $\delta^{15}N^{\beta}$ respectively (Fig. 2, left panels). The average linearized trends are (–0.032±0.004) ‰ a^{-1} for $\delta^{15}N$, (–0.014±0.008) ‰ a^{-1} for $\delta^{18}O$, (–0.019±0.015) ‰ a^{-1} for $\delta^{15}N^{\alpha}$ and (–0.041±0.020) ‰ a^{-1} for $\delta^{15}N^{\beta}$. These overall trends are slightly lower compared to previous studies that used

Atmos. Chem. Phys. Discuss., doi:10.5194/acp-2016-487, 2016
Manuscript under review for journal Atmos. Chem. Phys.
Published: 21 June 2016

only the data at individual sites (Ishijima et al., 2007; Bernard et al., 2006; Röckmann et al., 2003; Sowers et al., 2002) and other studies that used data from the same period, which were not used in the present study (Park et al., 2012). However, the differences lie well within the combined uncertainties. We note that comparisons of average linear trends can be flawed when the firn air records have different length and the temporal profiles do not change linearly (see below). Trends for $\delta^{15}N^{\alpha}$ are smaller in magnitude than for $\delta^{15}N^{\beta}$, while results from Bernard et al. (2006) showed stronger changes for $\delta^{15}N^{\alpha}$ than for $\delta^{15}N^{\beta}$. However, in that study the trends were largely determined from measurements on young ice core samples with comparatively higher measurement errors and scatter.

Data from two sites were not included in the multi-site inversion and are used as independent validation of the reconstructed scenarios. The data points from Ishijima et al. (2007) (NGRIP-01, yellow) are within the range of scenarios reconstructed by the inverse model and thus independently validate our results. The $\delta^{15}N^{av}$ and $\delta^{18}O$ data from Sowers et al. (2002) (SP-01 in light blue and SP-95 in blue) however, agree only for the more recent atmospheric history (Fig.2, left panels). For mean ages before 1990 most of the points are outside the uncertainty envelopes of the multi-site reconstruction. Inter-laboratory calibration differences might be a possible explanation for the discrepancy, but the differences are not a systematic shift, and they are larger than offsets among laboratories that were established in the past (Sapart et al., 2011; Kaiser et al., 2003). In fact, the data reported by Sowers et al., (2002) were actually measured with good agreement in two different laboratories.

To evaluate our scaling approach we repeated the multi-site reconstruction using the original non re-scaled data and the data that were re-scaled to NEEM-09 instead of DC-99 (see Appendix C). The data rescaled to NEEM-09 gave very similar results (within uncertainties) to the one re-scaled to DC-99 as was expected, thus the results do not depend on the choice of the site used for re-scaling. Without re-scaling, the overall change of N_2O mole fraction and isotopic composition remained the same, but an additional decadal variability was introduced for $\delta^{15}N^{av}$, $\delta^{15}N^{\alpha}$ and $\delta^{15}N^{\beta}$. In addition to that, the uncertainty envelopes doubled because of the scale inconsistencies. All scaling approaches produce results that are consistent with our preferred scaling to DC-99 within the uncertainty envelopes. We conclude that DC-99 re-scaling removed the discrepancies that would cause larger errors if the original data were used instead, but the re-scaling does not introduce artificial signals (see Appendix C).

Atmos. Chem. Phys. Discuss., doi:10.5194/acp-2016-487, 2016
Manuscript under review for journal Atmos. Chem. Phys.
Published: 21 June 2016

Atmospheric Chemistry and Physics Discussions

The regularization of the inversion results using a rugosity factor introduces a free parameter, which is chosen to eliminate overfitting of experimental uncertainties and which controls the smoothness of the reconstruction. The value of this parameter is set based on a robust generalized cross validation criterion, ensuring that the resolution obtained from the inverse model is similar to the experimental data while taking into account the sparsity of the measurements (Witrant and Martinerie, 2013). A sensitivity experiment where the weight of the regularization term is increased, which leads to comparable results as linear tropospheric histories presented in Fig. 2 was performed (Appendix C). This combined with the fact that straight lines can be drawn within the uncertainty envelopes of the reconstructed scenarios and the sensitivity tests (see Appendix C) indicates that the isotopic trends are not significantly different from straight lines within the current uncertainties.

3.3 Reconstruction of the N_2O emission history

Fig. 3 shows the temporal evolution of the global N_2O mole fraction as inferred from the firn air reconstruction in the top panel, and in the bottom panel the emission strength in Tg a^{-1} N calculated with the mass balance model (Section 2.5). The solid black line denotes the best estimate scenario, which is used as input in the mass balance model. The magenta lines show the ensemble of random scenarios generated to quantify the uncertainty of the emissions (see Section 2.6).

The increase in the N_2O mole fraction of (32±1) nmol mol^{-1} over the reconstruction period can be explained in the mass balance model by an increase in the emissions from (11.9±1.7) Tg a^{-1} N in 1940 to (16.4±1.7) Tg a^{-1} N in 2008. The emissions increased with an increasing trend until 1975, then the annual increase continued, but at a slower rate up to 1990, and from then on the annual emissions have stayed approximately constant or even decreased slightly. The corresponding changes in the mole fraction (increasing growth rate before 1990, no increase and possibly slight decrease in the growth rate afterwards) are difficult to discern due to the long atmospheric lifetime of N_2O. On average, the annual growth rate from 1995 to 2008 period is 0.7 nmol mol^{-1} a^{-1}, corresponding to average annual emissions of 3.5 Tg a^{-1} N.

3.4 The temporal evolution of the N_2O isotope signatures

The results from the isotope budget calculations are presented in Fig. 4. The left panels show the atmospheric trends. The solid black lines represent the best-fit scenarios while the dashed black lines represent the upper and lower uncertainty envelope of the firn air reconstructions.

Atmos. Chem. Phys. Discuss., doi:10.5194/acp-2016-487, 2016
Manuscript under review for journal Atmos. Chem. Phys.
Published: 21 June 2016

The magenta lines represent 50 scenarios generated randomly within the reconstructed uncertainty range, as described in section 2.6. The middle panels show the temporal changes in the isotope signatures of the total N_2O source, with their accompanied uncertainties, as calculated from the atmospheric mass balance model (section 2.5). The total source is split into an assumed constant "natural" and an increasing "anthropogenic" component and the right panels show the isotopic evolution of the "anthropogenic" component.

Results show that the average $\delta^{15}N^{av}$ of the total N_2O source, over the reconstruction period, is (–7.6±0.6) ‰ where the uncertainty is calculated using the 1σ uncertainty from the scenarios with respect to the mean value (magenta lines). There is no statistically significant long-term trend, but a temporal variability is observed on the decadal scale that might mask this trend. $\delta^{15}N^{av}$ first decreased from (–6.5±0.6) ‰ in 1940 to (–8.5±0.6) ‰ in 1965, then slowly increased again to (–6.6±0.6) ‰ in 1985, followed by another decrease to (–8.5±0.6) ‰ in 2008. These oscillations originate from the slightly curved trends in the isotopic reconstructions for $\delta^{15}N^{av}$ in Fig. 5 (left panels).

When the source is split into a constant natural and a varying anthropogenic component, the variability is primarily projected on the anthropogenic part and the temporal variations increase accordingly. However, also the uncertainties increase substantially, because the differences between the individual scenarios are attributed to only a small fraction of the total source.

The $\delta^{15}N^{av}$ signature of the anthropogenic source has an average value of (–18.2±2.6) ‰. It initially increases (the small initial decrease is not significant) from (–21.5±2.6) ‰ in 1940 to (–8.6±2.6) ‰ in 1990 where it starts to slowly decrease reaching (–15.4±2.6) ‰ in 2008. During the early part of the reconstruction period (<1970), when the "anthropogenic" contribution was only a small fraction of the total source, the uncertainty ranges of the source signatures are large. Therefore, the uncertainties for the early part (<1970) were excluded from the uncertainty 1σ uncertainties from the generated scenarios. This applies to all anthropogenic isotope signatures.

The budget calculations suggest an overall trend towards more enriched anthropogenic emissions but the uncertainties are very large. Mathematically, this trend arises from the fact that the isotope reconstructions yield relatively linear temporal isotope trends, whereas the source strength increases in a strongly non-linear fashion (Fig. 4). In the beginning of the record a small increase in the source strength needs to produce a similar absolute isotope shift

Atmos. Chem. Phys. Discuss., doi:10.5194/acp-2016-487, 2016
Manuscript under review for journal Atmos. Chem. Phys.
Published: 21 June 2016

Atmospheric Chemistry and Physics Discussions

as a larger increase in the source strength in later years. This can only be satisfied by a lower $\delta^{15}N^{av}$ value for the small "anthropogenic" emissions in the early part of the firn record. A constant $\delta^{15}N^{av}$ source signature would result in a small temporal change in $\delta^{15}N^{av}$ of atmospheric N_2O in the beginning of the record and increasing isotope trends with increasing emissions, similar to the exponential curves that were fit to the firn air data in Röckmann et al. (2003).

The $\delta^{18}O$ of the total source varies within (27.2±2.6) ‰ over the entire period. $\delta^{18}O$ does not show significant decadal scale oscillations because the reconstructed scenario for $\delta^{18}O$ is even more strictly linear than the $\delta^{15}N^{av}$ scenario. For this reason, as explained above, in the best fit scenario the $\delta^{18}O$ of the anthropogenic source for the initial 30 years has a more depleted value starting with (15.2±2.6) ‰ in year 1940, reaching (31.1±2.6) ‰ in year 1975 and remaining around this value until 2008 (Fig. 5). However, the relatively larger uncertainty envelopes for the atmospheric history of $\delta^{18}O$ actually allow scenarios with smaller $\delta^{18}O$ changes in the beginning of the record and larger changes in the later period, which means that the reconstruction does not exclude a constant value for the anthropogenic $\delta^{18}O$ source signature. The available dataset thus does not allow quantifying a long-term trend in $\delta^{18}O$.

For the position dependent ^{15}N signatures of the total source no significant long-term trends were detected. For $\delta^{15}N^{\alpha}$ no decadal scale variability is observed, whereas for $\delta^{15}N^{\beta}$ a temporal variability is observed similar to the $\delta^{15}N^{av}$. The uncertainty ranges for $\delta^{15}N^{\alpha}$ and $\delta^{15}N^{\beta}$ are about a factor 2 greater than for $\delta^{15}N^{av}$, which is due to the larger analytical error that leads to higher uncertainties in the scenario reconstructions. $\delta^{15}N^{\alpha}$ varies in the range (–3.0±1.9) ‰, $\delta^{15}N^{\beta}$ in the range (–11.7±2.3) ‰.

The temporal evolution of $\delta^{15}N^{\alpha}$ of the anthropogenic source looks similar to that of $\delta^{18}O$, but with even larger variations and uncertainties with a total average of (–8.1±1.7) ‰. $\delta^{15}N^{\alpha}$ increased from (–18.2±1.7) ‰ in 1940 to an average of (-5.4±1.7) ‰ in 1975 and retained this value until 2008. In contrast, $\delta^{15}N^{\beta}$ is similar to that of $\delta^{15}N^{av}$ with a total anthropogenic source average of (–26.1±8.4). $\delta^{15}N^{\beta}$ initially decreases from (–19.1±8.4) ‰ to (-42.0±8.4) ‰ in 1955 only to increase again to (-10.6±8.4) ‰ in year 1990 and then decrease again to (-26.0±8.4) ‰ in 2008.

Atmos. Chem. Phys. Discuss., doi:10.5194/acp-2016-487, 2016
Manuscript under review for journal Atmos. Chem. Phys.
Published: 21 June 2016

Atmospheric Chemistry and Physics Discussions

4 Discussion

From the combination of the firn air reconstruction with a simple two-box model we conclude that N_2O emissions increased from (11.9±1.7) Tg a^{-1} N in 1940 to (16.4±1.7) Tg a^{-1} N in 2008. This agrees, within uncertainties, with previous firn reconstruction studies from Ishijima et al. (2007) and Park et al. (2012) and bottom-up approaches using emission databases (Syakila and Kroeze, 2013; Kroeze et al., 1999). A more recent study by Thompson et al. (2014b) performed inversions of atmospheric measurements for 2006 to 2008 with multiple models and reported emissions of 16.1-18.7 Tg a^{-1} N for 2008 in agreement with our findings.

To investigate the effect of lifetime choice on the N_2O isotopic signatures (Prather et al. (2015) we performed a sensitivity study where we linearly changed the N_2O lifetime from 123 years pre-industrially (≈1750) to 119 years in modern times (2008). The results are shown in Appendix D, where the effect on the emission strength and isotopic composition is discussed in detail. Results from this sensitivity study showed that the effect of a decreasing lifetime gives higher N_2O emissions for year 2008 while keeping the same pre-industrial value, confirming a sensitivity in the choice of lifetime in line with Prather et al. (2015). Consequently this sensitivity only influences the anthropogenic isotopic signature by 10 %, meaning that the resulting values can increase by (2.0±1.0) ‰. The lifetime effect is most pronounced for the earliest part of the record (<1970) where the reconstruction uncertainties are larger than this systematic uncertainty.

The increase in N_2O emissions over the past decades resulted in an overall decrease of all isotopic signatures of atmospheric N_2O with time. The isotopic signature of the total source of N_2O (Fig. 4, middle panels) is strongly depleted in all heavy isotopes compared to tropospheric N_2O (Table 3), which is due to the strong enrichment associated with the removal in the stratosphere. In Table 3 the isotopic composition for the pre-industrial period (≈1750) ($\delta_{nat,pi}$) is compared with the derived anthropogenic source signature derived from our multi-site reconstruction (δ_{anth}, averaged from 1940 to 2008). The results show that the anthropogenic source is more depleted in heavy isotopes than the natural one for all signatures, confirming results from previous studies that used forward firn air modelling on measurements from individual sites (Park et al., 2012; Ishijima et al., 2007; Röckmann et al., 2003).

Atmos. Chem. Phys. Discuss., doi:10.5194/acp-2016-487, 2016
Manuscript under review for journal Atmos. Chem. Phys.
Published: 21 June 2016

574 Anthropogenic N_2O emissions are dominated by agricultural soil (70 %) with smaller
575 contributions from automobiles, coal combustion, biomass burning and industry. Oceanic
576 emissions were previously assumed to be only natural. However, the latest IPCC Assessment
577 Report (IPCC, ch.6, 2013) for the first time breaks down oceanic emissions into a natural and
578 an anthropogenic component, e.g. due to atmospheric N deposition to rivers (Syakila and
579 Kroeze, 2011; Duce et al., 2008; Kroeze et al., 2005), thus estimating the anthropogenic
580 component of oceanic N_2O emissions to amount to 1 Tg a^{-1} N.

581 N_2O emitted from agricultural soils and biomass burning is more depleted in $\delta^{15}N$ and $\delta^{18}O$
582 than the tropospheric background (Park et al., 2011; Goldberg et al., 2010; Ostrom et al.,
583 2010; Tilsner et al., 2003; Perez et al., 2001; 2000) while N_2O emitted from other minor
584 sources, such as automobiles, coal combustion and industry, has values closer to tropospheric
585 N_2O values (Syakila and Kroeze, 2011; Toyoda et al., 2008; Ogawa and Yoshida, 2005a;
586 2005b).

587 Qualitatively, an increase of strongly depleted agricultural emissions in the first part of our
588 reconstruction, followed by a decreasing relative contribution from agriculture and increasing
589 contributions from more enriched sources like industry, automobiles and coal combustion,
590 can explain the reconstructed changes of isotope signatures of both the total source and the
591 anthropogenic component. The global N_2O budget study from Syakila and Kroeze (2011)
592 indicates that agricultural emissions were 78 % of the total during the 1940-1980 period with
593 little input from industry, vehicle exhaust and coal combustion. After 1980 the relative share
594 of agricultural emissions dropped to 64 %, while the other sources increased, supporting our
595 suggestion.

596 Additional evidence for potential changes in the N_2O source composition between the pre-
597 industrial and present atmosphere may be derived from the position-dependent ^{15}N signatures,
598 quantified by the ^{15}N site preference. Table 3 shows that the difference in the $\delta^{15}N^{av}$ signature
599 between the pre-industrial and the anthropogenic source derived from our reconstruction is
600 primarily due to a change at position $\delta^{15}N^{\beta}$, whereas $\delta^{15}N^{\alpha}$ remains relatively constant. This is
601 reflected by a larger difference in $\delta^{15}N^{sp}$ between natural and anthropogenic emissions, which
602 could indicate a temporal change in production processes.

603 Sutka et al. (2006) suggested that there may be two distinct classes of N_2O sources with
604 different $\delta^{15}N^{sp}$. N_2O produced during nitrification and fungal denitrification had a high $\delta^{15}N^{sp}$
605 of (33±5) ‰ and N_2O from denitrification and nitrifier denitrification had a low $\delta^{15}N^{sp}$ of

Atmos. Chem. Phys. Discuss., doi:10.5194/acp-2016-487, 2016
Manuscript under review for journal Atmos. Chem. Phys.
Published: 21 June 2016

Atmospheric Chemistry and Physics Discussions

606 (0±5) ‰. Park et al., (2012) used these two endmembers to calculate a change in the relative
607 fractions of these source classes over time based on their firn air data. Although this approach
608 is strongly simplified and several other sources and factors may contribute (Toyoda et al.,
609 2015), we use the results from our box model calculations (Table 3) in a similar way to
610 estimate the fraction of the two source categories according to the following simple mass
611 balance calculation:

612 $$F_{\mathrm{high}} = \frac{\delta^{15}\mathrm{N}^{\mathrm{sp}}_{\mathrm{meas}} - \delta^{15}\mathrm{N}^{\mathrm{sp}}_{\mathrm{low}}}{\delta^{15}\mathrm{N}^{\mathrm{sp}}_{\mathrm{high}} - \delta^{15}\mathrm{N}^{\mathrm{sp}}_{\mathrm{low}}} \qquad (11)$$

613 This returns a fractional contribution of the $\delta^{15}N^{sp}_{high}$ component of (19±4) % to the total pre-
614 industrial emissions and (35±11) % to the total present source. The errors were derived by
615 propagating the errors of the $\delta^{15}N^{sp}$. endmembers and $\delta^{15}N^{sp}_{meas}$ as given above. We note that
616 the errors associated with the precise isotopic composition of the endmembers are correlated
617 if $\delta^{15}N^{sp}$.for the two endmembers remain relatively constant. Therefore, the change in the
618 relative fraction of the two categories is likely better constrained than the absolute values.

619 Splitting the total present emission strength into a natural (pre-industrial, 11.0 Tg a^{-1} N) and
620 anthropogenic (5.4 Tg a^{-1} N) component, we derive a fraction of the $\delta^{15}N^{sp}_{high}$ component
621 (which includes nitrification) of (54±26) % for the "anthropogenic" emissions. This is another
622 piece of evidence for agricultural sources being the main contributor to the N_2O increase,
623 because nitrification-dominated agricultural emissions can be associated with the $\delta^{15}N^{sp}_{high}$
624 component.

625 The temporal changes of the derived fraction of nitrification are in good qualitative agreement
626 with the results from Park et al. (2012), who reported a change of (13±5) % from 1750 to
627 (23±13) % today. However, the absolute numbers derived from our study are higher than the
628 results from Park et al. (2012). The difference is due to the fact that different apparent isotope
629 fractionations during stratospheric removal (ε_{app}) are used in the mass balance model (Table
630 3; eq. 7,8). In this study we used the averaged lowermost stratospheric apparent isotope
631 fractionations from Kaiser et al. (2006), which we consider more representative than the
632 numbers used by Park et al. (2012). Using different values for ε_{app} causes a shift in the
633 isotopic source signatures from the mass balance model. The choice of this value thus adds a
634 systematic source of uncertainty to the absolute value of the $\delta^{15}N^{sp}_{high}$ fractions reported above
635 (F_{high}).

Atmos. Chem. Phys. Discuss., doi:10.5194/acp-2016-487, 2016
Manuscript under review for journal Atmos. Chem. Phys.
Published: 21 June 2016

636 Nevertheless, this systematic uncertainty should not alter the overall *change* in F_{high} from pre-
637 industrial to modern times and the results from our multi-site reconstruction of the isotopic
638 composition of N_2O thus confirm the suggestion by Park et al. (2012) that the relative
639 importance of the high-SP component (presumably nitrification) has increased with increasing
640 mole fraction since pre-industrial times.

641 ## 5 Conclusions

642 The temporal evolution of the total N_2O emission fluxes and the source isotopic composition
643 have been estimated in a top-down approach using a multi-site reconstruction of N_2O mole
644 fraction and isotopic composition from 6 firn air samplings at 5 different Arctic and Antarctic
645 locations in a two-box model. The results from a mass balance model constraints the source
646 strength and suggest a total increase in N_2O emissions of (4.5±1.7) Tg a^{-1} N between the 1940
647 and 2008 due to anthropogenic processes. This agrees with previous top-down estimates, but
648 deviates from bottom-up model estimates, which suggest higher N_2O emission increases. A
649 significant source of the uncertainty in such top-down estimates is a possible change in the
650 N_2O lifetime over the reconstruction period, which we have quantified following the recent
651 results from Prather et al. (2015).

652 The reconstruction of mole fraction and isotopic composition was used to investigate
653 temporal changes in the isotopic signature of N_2O emissions over the study period. The
654 average total source for $\delta^{15}N^{av}$ and $\delta^{15}N^{\beta}$ shows no statistically significant long-term trend but
655 likely significant decadal scale variability. For $\delta^{18}O$ and $\delta^{15}N^{\alpha}$ of the total N_2O source, no
656 significant temporal changes can be detected with the present dataset because the
657 uncertainties are large, especially in the beginning of the reconstruction period.

658 When the total source is split into a constant natural and a varying anthropogenic component,
659 the reconstruction of the δ values of the anthropogenic source indicates a significant increase
660 of $\delta^{15}N^{av}$ from the early to the modern part of the record. This originates from the near-linear
661 isotope histories of the best guess scenario, which would imply that small emissions in the
662 early part had a similar absolute effect on the δ values as stronger emissions in the latter part.
663 A similar effect for $\delta^{18}O$ is likely, but not significant given the larger uncertainties for this
664 signature.

665 Nevertheless, the isotope signal in $\delta^{15}N^{av}$ may also be a signal for changing source
666 contributions over time. Bottom-up models suggest that N_2O emitted from agricultural soils

Atmos. Chem. Phys. Discuss., doi:10.5194/acp-2016-487, 2016
Manuscript under review for journal Atmos. Chem. Phys.
Published: 21 June 2016

was the dominant contributor to the anthropogenic N_2O increase in the first decades. Smaller contributions due to emissions from more enriched sources, like industry, automobiles and coal combustion increased, which may have contributed to an isotope enrichment of the emissions, which is not detectable within the error bars for the other isotope signatures.

Results from the mass balance model yield an increase in ^{15}N site preference between the pre-industrial and modern total N_2O source. The increase in $\delta^{15}N^{sp}$ of (16±11) % between the pre-industrial and modern source is in qualitative agreement with increased emissions from nitrification processes associated with agriculture.

Acknowledgements

We thank the teams involved in the firn air sampling at NEEM site during the 2008 and 2009 field seasons. NEEM is directed and organized by the Centre of Ice and Climate at the Niels Bohr Institute, University of Copenhagen, Denmark and the US National Science Foundation, Office of Polar Programs. It is supported by funding agencies and institutions in Belgium (FNRS-CFB and FWO), Canada (NRCan/GSC), China (CAS), Denmark (FIST), France (IPEV, CNRS/INSU, CEA and ANR), Germany (AWI), Iceland (RannIs), Japan (NIPR), Korera (KOPRI), The Netherlands (NWO/ALW and NWO/NPP), the United Kingdom (NERC NE/F021194/1) and the USA (US NSF, Office of Polar Programs). This project was financially supported by the Dutch Science Foundation (NWO), projects 851.30.020 & 865.07.001.

References

Allin, S. J., Laube, J. C., Witrant, E., Kaiser, J., McKenna, E., Dennis, P., Mulvaney, R., Capron, E., Martinerie, P., Röckmann, T., Blunier, T., Schwander, J., Fraser, P. J., Langenferls, R. L., and Sturges, W. T.: Chlorine isotope composition in chlorofluorocarbons CFC-11, CFC-12 and CFC-113 in firn, stratospheric and tropospheric air, Atmos. Chem. Phys., 15, 6867-6877, doi:10.5194/acp-15-6867-2015, 2015.

Bernard, S., Röckmann, T., Kaiser, J., Barnola, J.-M., Fischer, H., Blunier, T., and Chappellaz, J.: Constraints on N_2O budget changes since pre-industrial time from new firn air and ice core isotope measurements, Atmos. Chem. Phys., 6,, 493–503, doi:10.5194/acp-6-493-2006, 2006.

Buizert, C., Sowers, T., and Blunier, T.: Assessment of diffusive isotopic fractionation in polar firn, and application to ice core trace gas records, Earth Planet. Sci. Lett., 361, 110–119, 2013.

Butterbach-Bahl, K., and Dannenmann, M.: Denitrification and associated soil N_2O emissions due to agricultural activities in a changing climate, Curr. Op. Environ. Sus., 3(5), 389–395, doi:10.1016/j.cosust.2011.08.004, 2011.

Ciais, P., Sabine, C., Bala, G., Bopp, L., Brovkin, V., Canadell, J., Chhabra, A., DeFries, R., Galloway, J., Heimann, M., Jones, C., Le Quéré, C., Myneni, R.B., Piao, S., and Thornton, P.: Carbon and other biogeochemical cycles. Climate Change 2013: The Physical Science Basis, Contribution of Working Group I to the Fifth Assessmetn Report of the Intergovernmental Panel on Climate Change, Cambridge University Press, Cambridge, United Kingdom and New York, NY, USA, 2013.

Crutzen, P. J., Mosier, A. R., Smith, K. A., and Winiwarter, W.: N_2O release from agro-biofuel production negates global warming reduction by replacing fossil fuels, Atmos. Chem. Phys., 8, 389-395, doi:10.5194/acp-8-389-2008, 2008.,

Davidson, E. A.: The contribution of manure and fertilizer nitrogen to atmospheric nitrous oxide since 1860, Nat. Geosci., 2(9), 659–662, doi:10.1038/ngeo608, 2009.

713 Duce, R. A., LaRoche, J., Altieri, K., Arrigo, K .R., Baker, A. R., Capone, D. G., Cornell, S.,
714 Dentener, F., Galloway, J., and Ganeshram, R. S.: Impacts of atmospheric anthropogenic
715 nitrogen on the open ocean, Science, 320, 893-897, 2008.

716 Freing, A., Wallace, D. W. R., and Bange, H. W.: Global oceanic production of nitrous oxide,
717 Phil. Trans. R. Soc. Lond., Series B, 367(1593), 1245–55, doi:10.1098/rstb.2011.0360, 2012.

718 Hirsch, A., Michalak, A., Bruhwiler, L., Peters, W., Dlugokencky, E., and Tans, P.: Inverse
719 modelling estimates of the global nitrous oxide surface flux from 1998-2001, Gl. Biochem.
720 Cycl., 20, GB 1008, doi: 10.1029/2004GB002443, 2006.

721 Holton, J. R.: On the global exchange of mass between stratosphere and troposphere, J.
722 Atmos. Sci. , 47(3), 392-395, 1990.

723 Houghton, J. T., Meira Filho, L. G., Bruce, J., Lee, H., Callander, B. A, Haites, E., Harris, N.,
724 and Maskell, K.: Climate Change 1994: Radiative Forcing of Climate Change and an
725 Evaluation of the IPCC IS 92 Emission Scenarios, Cambridge University Press, Cambridge,
726 UK, 1994.

727 Ishijima, K., Sugawara, S., Kawamura, K., Hashida, G., Morimoto, S., Murayama, S., Aoki,
728 S.: Temporal variations of the atmospheric nitrous oxide concentration and its $\delta^{15}N$ and $\delta^{18}O$
729 for the latter half of the 20th century reconstructed from firn air analyses, J. Geophys. Res.,
730 112(D3), doi:10.1029/2006JD007208, 2007.

731 Kaiser, J., Brenninkmeijer, C.A.M., Röckmann, T.: Intramolecular ^{15}N and ^{18}O fractionation
732 in the reaction of N_2O with $O(^1D)$ and its implications for the stratospheric N_2O isotopic
733 signature, J. Geophys. Res., 107 (4214), doi:10.1029/2001JD001506, 2002.

734 Kaiser, J., Röckmann T., and Brenninkmeijer, C.A.M.: Complete and accurate mass
735 spectrometric isotope analysis of tropospheric nitrous oxide, J. Geophys. Res., 108(D15), 1–
736 17, doi:10.1029/2003JD003613, 2003.

737 Kaiser, J., Engel, A., Borchers, R., and Röckmann, T.: Probing stratospheric transport and
738 chemistry with new balloon and aircraft observations of the meridional and vertical N_2O
739 isotope distribution, Atmos. Chem. Phys., 6, 3535-3556, doi:10.5194/acp-6-3535-2006, 2006.

740 Kaiser, J., and Röckmann T.: Correction of mass spectrometric isotope ratio measurements
741 for isobaric isotopologues of O_2 ,CO, CO_2, N_2O and SO_2, Rap. Commun. Mass Spec., 3997–
742 4008, doi: 10.1002/rcm.3812, 2008.

743 Kim, K. R., and Craig, H.: Nitrogen-15 and Oxygen-18 Characteristics of Nitrous Oxide: A
744 global perspective, Science, 262, 1855-1857, 1993.

745 Kim, K. R., Craig, H.: Two-isotope characterization of N_2O in the Pacific Ocean and
746 constraints on its origin in deep water, Nature, 347, 58-61, doi:10.1038/347058a0, 1990.

747 Kool, D. M., Wrage, N., Oenema, O., Harris, D., and Groenigen, J. W. Van.: The ^{18}O
748 signature of biogenic nitrous oxide is determined by O exchange with water, Rap. Commun.
749 Mass Spec., 104–108, doi:10.1002/rcm.3859, 2009.

750 Kroeze, C., Mosier, A., and Bouwman, L.: Closing the global N_2O budget: a retrospective
751 analysis 1500-1994, Glob. Biogeochem. Cycl., 13, 1-8, doi: 10.1029/1998GB900020, 1999.

752 Kroeze, C., Dumont, E., and Seitzinger, S. P.: New estimates of global emissions of N_2O from
753 rivers and estuaries, Environ. Science, 2, 159-165, doi:10.1080/15693430500384671, 2005.

754 Löscher, C.R., Kock, A., Könneke, M., LaRoche, J., Bange, H. W., and Schmitz, R. A.:
755 Production of oceanic nitrous oxide by ammonia-oxidizing archaea, Biogeosciences, 9, 2419-
756 2429, doi:10.5194/bg-9-2419-2012, 2012.

757 Maeda, K., Toyoda, S., Shimojima, R., Osada, T., Hanajima, D., Morioka, R., and Yoshida,
758 N.: Source of nitrous oxide emissions during the cow manure composting process as revealed
759 by isotopomer analysis of and amoA abundance in betaproteobacterial ammonia-oxidizing
760 bacteria, Appl. Environ. Microbiol., 76(5), 1555–62, doi:10.1128/AEM.01394-09, 2010.

761 Martinerie, P., Nourtier-Mazauric, E., Barnola, J.-M., Sturges, W. T., Worton, D. R., Atlas,
762 E., Brasseur, G. P.: Long-lived halocarbon trends and budgets from atmospheric chemistry
763 modelling constrained with measurements in polar firn, Atmos. Chem. Phys, 9, 3911-3934,
764 doi:10.5194/acp-9-3911-2009, 2009.

765 McLinden, C. A., Prather, M. J., Johnson M. S.: Global modeling of the isotopic analogues of
766 N_2O: Stratospheric distributions, budgets and the ^{17}O-^{18}O mass-independent anomaly, J.
767 Geophys. Res., 108(D8), doi:10.1029/2002JD002560, 2003.

768 Minschwaner, K., Salawitch, R.J., McElroy, M.B.: Absorption of Solar Radiation by O_2:
769 Implications for O_3 and lifetimes of N_2O, $CFCl_3$, and CF_2Cl_2, J. Geophys. Res., 98, 10543-
770 10561, doi: 10.1029/93JD00223, 1993.

771 Ogawa, M., and Yoshida, N.: Intramolecular distribution of stable nitrogen and oxygen
772 isotopes of nitrous oxide emitted during coal combustion, Chemosphere, 61, 877-887, 2005a.

773 Ogawa, M., and Yoshida, N.: Nitrous oxide emission from the burning of agricultural residue.
774 Atmos. Environ., 39, 3421-3429, 2005b.

775 Ostrom, N. E., and Ostrom, P. H.: The isotopomers of Nitrous Oxide: Analytical
776 considerations and application to resolution of microbial production pathways, Baskaran, M.,
777 Handbook of Environmental Isotope Geochemisttry, Advances in Isotope Geochemistry,
778 Springer, Verlag, Berlin, Heidelberg, 453-476, 2011.

779 Park, S., Atlas, E. L., and Boering, K. A.: Measurements of N_2O isotopologues in the
780 stratosphere: Influence of transport on the apparent enrichment factors and the isotopologue
781 fluxed to the troposphere, J. Geophys. Res., 109, doi:10.1029/2003JD003731, 2004.

782 Park, S., Croteau, P., Boering, K. A., Etheridge, D. M., Ferretti, D., Fraser, P. J., and
783 Trudinger, C. M.: Trends and seasonal cycles in the isotopic composition of nitrous oxide
784 since 1940, Nat. Geosci., *5*(4), 261–265, doi:10.1038/ngeo1421, 2012.

785 Pérez, T., Trumbonre, S. E, Tyler, S. C., Davidson, E. A., Keller, M., and Camargo, P. de.:
786 Isotopic variability of N_2O emissions from tropical forest soils, Glob, Biogeochem. Cycl.,
787 14(2), 525-535, 2000.

788 Pérez, T., Trumbore, S. E., Tyler, S. C., Matson, P. A, Ortiz-Monasterio, I., Rahn, T., and
789 Griffith, D. W. T.: Identifying the agricultural imprint on the global N_2O budget using stable
790 isotopes, J. Geophys. Res.,106(D9), 9869-9878, 2001.

791 Popp, B. N., Westley, M. B., Toyoda, S., Miwa, T., Dore, J. E, Yoshida, N., Rust, T. M.,
792 Sansone, F. J, Russ, M. E, Ostrom, N. E., and Ostrom, P. H: Nitrogen and oxygen
793 isotopomeric constraints on the origins and sea-to-air flux of N_2O in the oligotrophic
794 subtropical North Pacific gyre, Glob, Biogeochem. Cycl., 16, 1064,
795 doi:10.1029/2001GB001806, 2002.

796 Potter, K. E.: Nitrous oxide (N_2O) isotopic composition in the troposphere: instrumentation,
797 observations at Mace Head, Ireland, and regional modeling, PhD thesis, Department of Earth,
798 Atmospheric, and Planetary Sciences at the Massachusetts Institute of Technology, 2011.

799 Prather, M. J., et al.: Measuring and modeling the lifetime of nitrous oxide including its
800 variability, J. Geophys. Res. Atmos., 120, 5693-5705, doi: 10.1002/2015JD023267, 2015.

801 Ravishankara, A. R., Daniel, J. S., and Portmann, R. W.: Nitrous oxide (N_2O): the dominant
802 ozone-depleting substance emitted in the 21st century, Science, 326(5949), 123–125,
803 doi:10.1126/science.1176985, 2009.

804 Röckmann, T., Kaiser, J., Brenninkmeijer, C. A. M., Crowley, J. N., Borchers, R., Brand, W.
805 A., and Crutzen, J.: Isotopic enrichment of nitrous oxide ($^{15}N^{14}NO$, $^{14}N^{15}NO$, $^{14}N^{14}N^{18}O$) in
806 the stratosphere and in the laboratory, J. Geophys. Res., 106(D10), 10403-10410,
807 doi:10.1029/2000JD900822, 2001.

808 Röckmann, T., Kaiser, J., Brenninkmeijer, C. A. M., and Brand, W. A.: Gas
809 chromatography/isotope-ratio mass spectrometry method for high-precision position-
810 dependent ^{15}N and ^{18}O measurements of atmospheric nitrous oxide, Rap. Commun. Mass
811 Spectrom. , 17(16), 1897–1908, doi:10.1002/rcm.1132, 2003.

812 Röckmann, T., Kaiser, J., Brenninkmeijer, C. A. M.: The isotopic fingerprint of the pre-
813 industrial and the anthropogenic N_2O source, Atmos. Chem. Phys., 3, 315-323,
814 doi:10.5194/acp-3-315-2003, 2003.

815 Röckmann, T., and Levin, I.: High-precision determination of the changing isotopic
816 composition of atmospheric N_2O from 1990 to 2002, J. Geophys. Res., 110(D21), 1–8,
817 doi:10.1029/2005JD006066, 2005.

818 Santoro, A. E., Buchwald, C., Mcllvin, M. R., and Casciotti, K. L.: Isotopic signature of N_2O
819 produced by marine ammonia-oxidizing archaea,Science, 333(6047), 1282–1285,
820 doi:10.1126/science.1208239, 2011.

821 Sapart, C. J., van der Veen, C., Vigano, I., Brass, M., van de Wal, R. S. W., Bock, M.,
822 Fischer, H., Sowers, T., Buizert, C., Sperlich, P., Blunier, T., Behrens, M., Schmitt, J., Seth,
823 B., and Röckmann, T.: Simultaneous stable isotope analysis of methane and nitrous oxide of
824 ice core samples, Atmos. Meas. Tech., 4, 2607–2618, doi:10.5194/amt-4-2607-2011, 2011.

825 Sapart, C. J., Martinerie, P., Witrant, E., Chappellaz, J., van de Wal, R. S. W., Sperlich, P.,
826 van der Veen, C., Bernard, S., Sturges, W. T., Blunier, T., Schwander, J., Etheridge, D.,
827 Röckmann, T.: Can the carbon isotopic composition of methane be reconstructed from multi-
828 site firn air measurements?, Atmos. Chem. Phys., 13, 6993-7005, doi:10.5194/acp-13-6993-
829 2013, 2013.

830 Stocker, T. F., Qin, D., Plattner, G.-K., Tingor, M., Allen, S. K., Boschung, J., Nauels, A.,
831 Xia, Y., Bex, V., Midgley, P. M. et al.: IPCC, 2013: Climate Change 2013: The physical
832 Science Basis. Contribution of Working Group I to the Fifth Assessment Report of the
833 Intergovernmental Panel on Climate Change, Cambridge University Press, Cambridge, United
834 Kingdom and New York, NY, USA, 2013.

835 Sowers, T., Rodebaugh, A., Yoshida, N., and Toyoda, S.: Extending records of the isotopic
836 composition of atmospheric N_2O back to 1800 A.D. from air trapped in snow at the South
837 Pole and the Greenland Ice Sheet Project II ice core, Global Biogeochemical Cycles, 16(4),
838 1–10, doi: 10.1029/2002GB001911, 2002.

839 SPARC, 2013: SPARC Report on the Lifetimes of Stratospheric Ozone-Depleting
840 Substances, Their Replacements, and Related Species, edited by: Ko, M., Newman, P.,
841 Reimann, S., and Strahan, S, SPARC Report No. 6, WCRP-15, Zurich, Switzerland, 2013.

842 Suntharalingam, P., Buitenhuis, E., Le Quéré, C., Dentener, F., Nevison, C., Butler, J. H., and
843 Forster, G.: Quantifying the impact of anthropogenic nitrogen deposition on oceanic nitrous
844 oxide, Geophysical Research Letters, 39, doi:10.1029/2011GL050778, 2012.

845 Sutka, R. L., Ostrom, N. E., Ostrom, P. H., Breznak, J. A., Gandhi, H., Pitt, A. J., and Li, F.:
846 Distinguishing Nitrous Oxide Production from Nitrification and Denitrification on the Basis

847 of Isotopomer Abundances, Appl. Environ. Microbiol., 72(1), 638–644,
848 doi:10.1128/AEM.72.1.638-644.2006, 2006.

849 Syakila, A., Kroeze, C., and Slomp, C. P.: Neglecting sinks for N_2O at the earth's surface:
850 does it matter?, Journal of Integrative Environmental Sciences, 7, 79-87,
851 doi:10.1080/1943815X.2010.497492, 2010.

852 Syakila, A., and Kroeze, C.: The global nitrous oxide budget revisited, Greenhouse Gas
853 Measurement and Management, 1(1), 17–26, doi:10.3763/ghgmm.2010.0007, 2011.

854 Thompson, R. L., Ishijima, K., Saikawa, E., Corazza, M., Karstens, U., Patra, P. K.,
855 Bousquet, P. (2014). TransCom N_2O model inter-comparison, Part II: Atmospheric inversion
856 estimates of N_2O emissions. *Atmospheric Chemistry and Physics Discussions*, *14*(4), 5271–
857 5321.

858 Thompson, R. L., Patra, P. K., Ishijima, K., Saikawa, E., Corazza, M., Karstens, U.,
859 Bousquet, P.: TransCom N_2O model inter-comparison – Part 1: Assessing the influence of
860 transport and surface fluxes on tropospheric N_2O variability, Atmos. Chem. Phys. 14, 4349-
861 4368, doi:10.5194/acp-14-4349-2014, 2014.

862 Toyoda, S., Yamamoto, S., Arai, S., Nara, H., Yoshida, N., Kashiwajura, K., and Akiyama,
863 K.: Isotopomeric characterization of N_2O produced, consumed and, emitted by automobiles.,
864 Rap. Comm. in Mass Spec., 22, 603-612, doi:10.1002/rcm.3400, 2008.

865 Witrant, E., Martinerie, P., Hogan, C., Laube, J.C, Kawamura, K., Capron, E., Montzka, S.
866 A., Dlugokencky, E. J., Etheridge, D., Blunier, T., and Sturges, W. T.: A new multi-gas
867 constrained model of trace gas non-homogeneous transport in firn: evaluation and behavior at
868 eleven polar sites, Atmos. Chem. Phys., 12, 11465-11483, doi:10.5194/acp-12-11465-2012,
869 2012.

870 Witrant, E., Martinerie, P.: Input estimation from sparse measurements in LPV systems and
871 isotopic ratios in polar firn, IFAC Joint conferenc SSSC - 5th Symposium on System
872 Structure and Control, Grenoble, France, 150, 2013.

873 Westley, M. B., Popp, B. N., and Rust, T. M.: The calibration of the intramolecular isotope
874 distribution in nitrous oxide measured by isotope ratio mass spectrometry, Rap. Comm. in
875 Mass. Spec., 21(3), 391-405, doi:10.1002/rcm.2828, 2007.

876 Yoshida, N., and Toyoda, S.: Constraining the atmospheric N_2O budget from intramolecular
877 site preference in N_2O isotopomers, Nature, 405, 330–334, doi:10.1038/35012558, 2000.

878

879

880

Atmos. Chem. Phys. Discuss., doi:10.5194/acp-2016-487, 2016
Manuscript under review for journal Atmos. Chem. Phys.
Published: 21 June 2016

Atmospheric Chemistry and Physics Discussions

881 Table 1. Site information on the drilling locations of the North Greenland Ice core Project
882 (NGRIP-01), Berkner Island (BKN-03), North Greenland Eemian Ice drilling Project
883 (NEEM-EU-08, NEEM-09), Dome Concordia (DC-99) and Dronning Maud Land (DML-98),
884 where firn air samples were collected, and two key meteorological variables of each site.

Site	Location	Mean annual temperature (°C)	Surface accumulation rate (water equivalent) (cm a^{-1})	Sampling year
NGRIP-01	75° N 42° W	-31	20	2001
BKN-03	79° S 45° W	-26	13	2003
NEEM-EU-08	77.4° N 51.1° W	-29	22	2008
NEEM-09	77.4° N 51.1° W	-29	22	2009
DC-99	75° S 123° E	-53	3	1999
DML-98	75° S 65° E	-38	6	1998

885

886 Table 2. Detailed information in the mole fraction and the isotopic composition of the
887 laboratory reference gases used for correcting each set of firn air samples.

Site	Sampling year	Mole fraction (nmol mol^{-1})	$\delta^{15}N^{av}$ (‰)	$\delta^{18}O$ (‰)	$\delta^{15}N^{\beta}$ (‰)	$\delta^{15}N^{\alpha}$ (‰)
NGRIP-01	2001	318	6.64	44.61	-2.79	16.07
BKN-03	2003	318	6.64	44.61	-2.79	16.07
NEEM-EU-08	2008	324	6.22	44.40	-3.08	15.52
NEEM-09	2009	318	6.38	44.92	-2.66	15.41
DC-99	1999	318	6.64	44.61	-2.79	16.07
DML-98	1998	318	6.64	44.61	-2.79	16.07

Atmos. Chem. Phys. Discuss., doi:10.5194/acp-2016-487, 2016
Manuscript under review for journal Atmos. Chem. Phys.
Published: 21 June 2016

Atmospheric Chemistry and Physics Discussions

888 Table 3. Stratospheric isotope fractionation (ε_{app}) used in the mass balance model, and
889 isotopic composition of the natural and anthropogenic source, and the respective results from
890 Park et al. (2012).

	ε_{app} (‰) this study*	ε_{app} (‰) Park et al., 2012*	$\delta_{atm,pi}$ (‰) Park et al., 2012	$\delta_{nat,pi}$ (‰) this study*	$\delta_{nat,pi}$ (‰) Park et al., 2012	δ_{anth} (‰) this study*	δ_{anth} (‰) Park et al., 2012**
$\delta^{15}N$	-16.2	-14.9	9.3±0.2	-5.2±0.2	-5.3±0.2	-18.2±2.6	-15.6±1.2
$\delta^{18}O$	-13.4	-13.3	45.5±0.2	33.1±0.2	32.0±0.2	27.2±2.6	32.0±1.3
$\delta^{15}N^{\alpha}$	-23.0	-22.4	18.8±1.0	-1.9±1.0	-3.3±1.0	-8.1±1.7	-7.6±6.2
$\delta^{15}N^{\beta}$	-9.4	-7.1	-0.6±1.1	-8.3±1.1	-7.5±1.1	-26.1±8.4	-20.5±7.1
$\delta^{15}N^{sp}$	-	-	19.4±1.5	6.4±1.5	4.2±1.5	18.0±8.6	13.1±9.4

891 *ε_{app} values used in this study are averaged values from the lower stratosphere from Kaiser et al. (2006) and ε_{app}
892 values from Park et al. (2012) were used from Park et al. (2004). $\delta_{atm,pi}$ values are from Park et al. (2012) who
893 also calculated $\delta_{nat,pi}$ and δ_{anth} in a two-box model. Here, the δ_{anth} values are the averaged values over the whole
894 investigated period.

895

896

897

898

899

900

Atmos. Chem. Phys. Discuss., doi:10.5194/acp-2016-487, 2016
Manuscript under review for journal Atmos. Chem. Phys.
Published: 21 June 2016

Atmospheric Chemistry and Physics Discussions

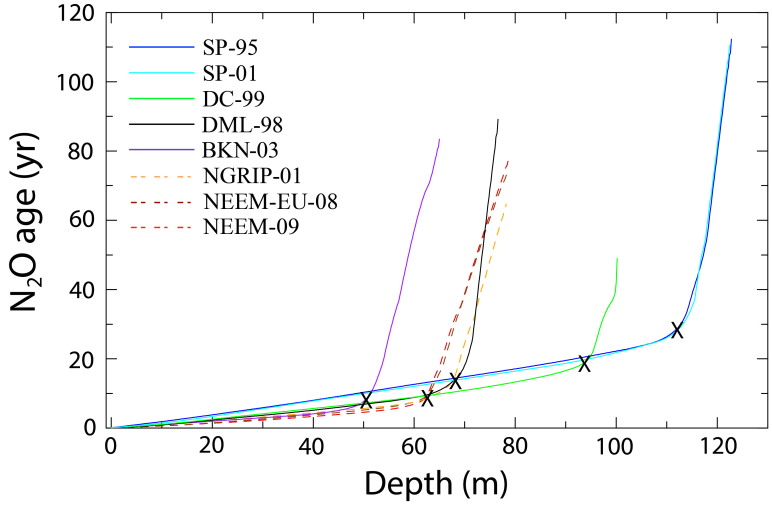

901

902 Figure 1. N_2O mean ages in firn versus depth. The dashed lines represent the sites from the
903 NH (North Greenland Ice-core Project [NGRIP-01], North Eemian Ice-core Project [NEEM-
904 09, NEEM-EU-08]) and the solid lines the SH sites (South Pole [SP-01, SP-95], Dome C
905 [DC-99], Dolomite [DML-98] and Berkner Island [BKN-03]). The numbers accompanying
906 the sites are the corresponding drilling years. Marker X indicates the transition between the
907 firn diffusive zone and the bubble close-off zone for each site. Dashed orange line NGRIP-01,
908 dashed brown NEEM-EU-08, dashed red NEEM-09, purple line BKN-03, black DML-98,
909 green DC-99, blue SP-95 and light blue SP-01.

Atmos. Chem. Phys. Discuss., doi:10.5194/acp-2016-487, 2016
Manuscript under review for journal Atmos. Chem. Phys.
Published: 21 June 2016

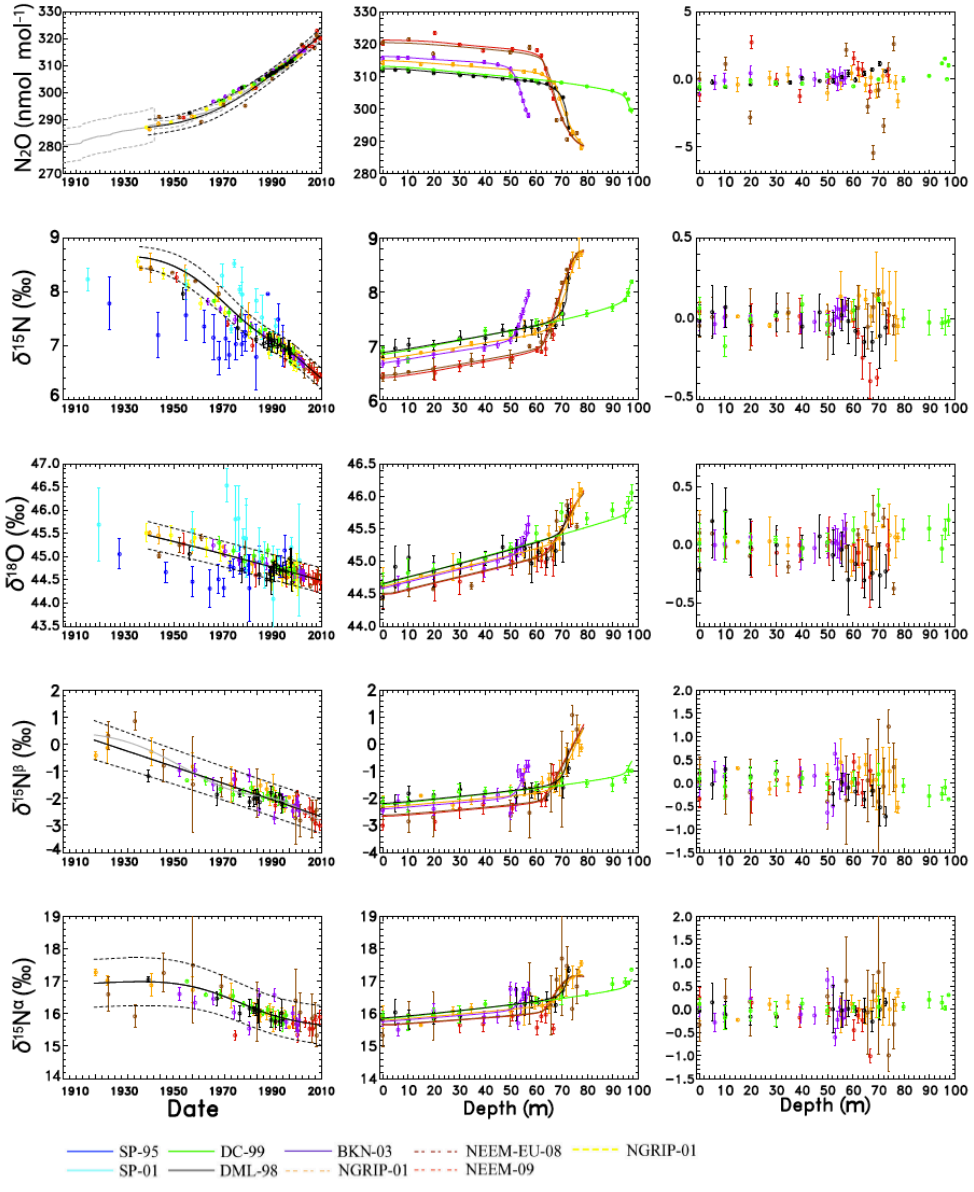

910

911

912

913

Atmos. Chem. Phys. Discuss., doi:10.5194/acp-2016-487, 2016
Manuscript under review for journal Atmos. Chem. Phys.
Published: 21 June 2016

Atmospheric Chemistry and Physics Discussions

914 Figure 2. Left: Reconstructed atmospheric scenarios (black solid line with dashed lines
915 indicating the 2 σ uncertainty intervals) and results of the firn air samples (corrected for firn
916 fractionation) plotted at their respective assigned mean age. Middle: corresponding depth
917 profiles, symbols show the measurements and solid lines the results of the forward model
918 using the best estimate scenario as input. Right: model data discrepancies. Orange: NGRIP-01
919 (Bernard et al, 2006), Yellow: NGRIP-01 (Ishijima et al., 2007), Brown: NEEM-EU-08, Red
920 NEEM-09, Purple: BKN-03, Black: DML-98, Green: DC-99, Blue: SP-95 and Light Blue:
921 SP-01. Data from NGRIP-01 (Ishijima et al., 2007), SP-95 and SP-01 were not used in the
922 atmospheric reconstruction and are only plotted for comparison purposes here.

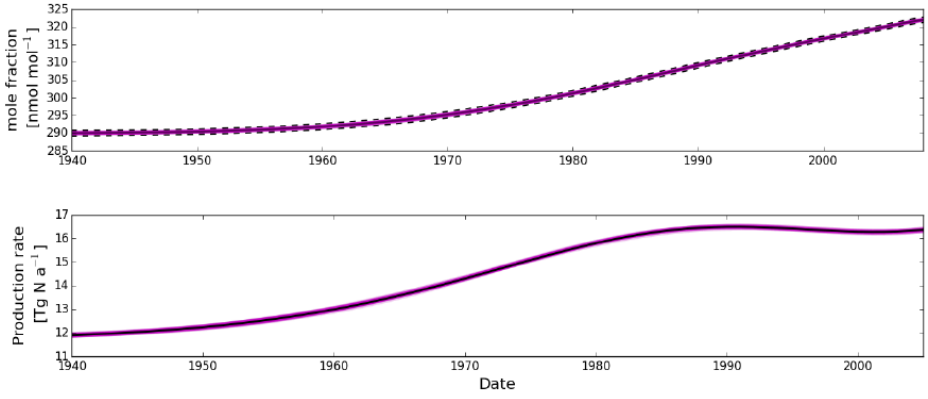

923

924 Figure 3: Top panel. N_2O mole fraction history from the multisite reconstruction (solid black
925 line with uncertainty envelopes as dashed black lines) and the scenarios within the uncertainty
926 envelopes that were used in the mass balance model (magenta lines) to evaluate the
927 uncertainties of the atmospheric modelling results.

928 Bottom panel. N_2O production rate as calculated from the mass balance model. The solid
929 black line represents the result for the best fit reconstruction while magenta lines represent the
930 results for the individual scenarios from the top panel.

931

932

Atmos. Chem. Phys. Discuss., doi:10.5194/acp-2016-487, 2016
Manuscript under review for journal Atmos. Chem. Phys.
Published: 21 June 2016

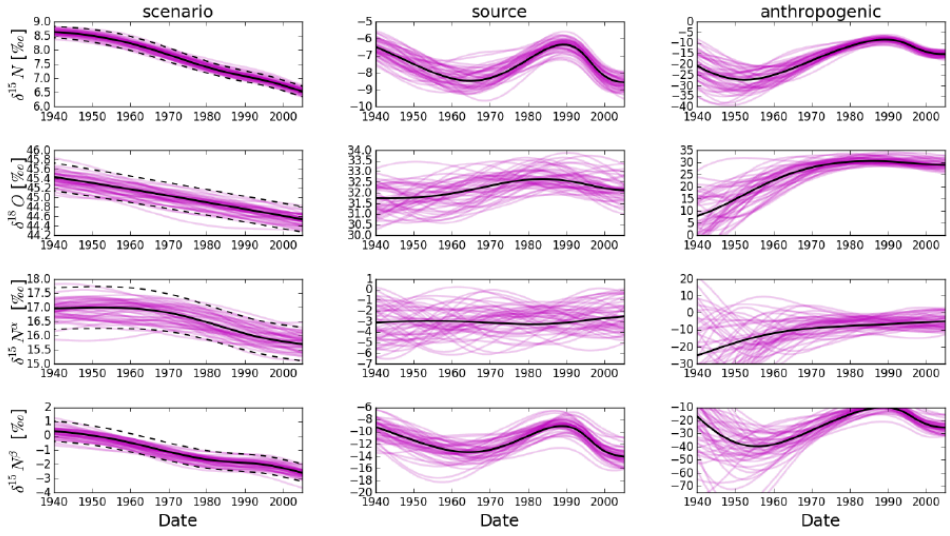

Figure 4: Left panels: Historic evolution of $\delta^{15}N$, $\delta^{18}O$, $\delta^{15}N^{\alpha}$ and $\delta^{15}N^{\beta}$ in N_2O as derived from the firn air reconstruction. Middle panels: isotope signatures of the total emitted N_2O. Middle panels: isotope signatures of the anthropogenic source, respectively. The solid black line represents the best-fit scenario while the dashed ones represent the respective uncertainties as determined by the reconstruction method. Magenta lines represent the emissions that are required to produce the magenta N_2O histories in the left panels.

Atmos. Chem. Phys. Discuss., doi:10.5194/acp-2016-487, 2016
Manuscript under review for journal Atmos. Chem. Phys.
Published: 21 June 2016

Atmospheric Chemistry and Physics Discussions

951 **Appendix A: Effect of firn fractionation on isotopic composition**

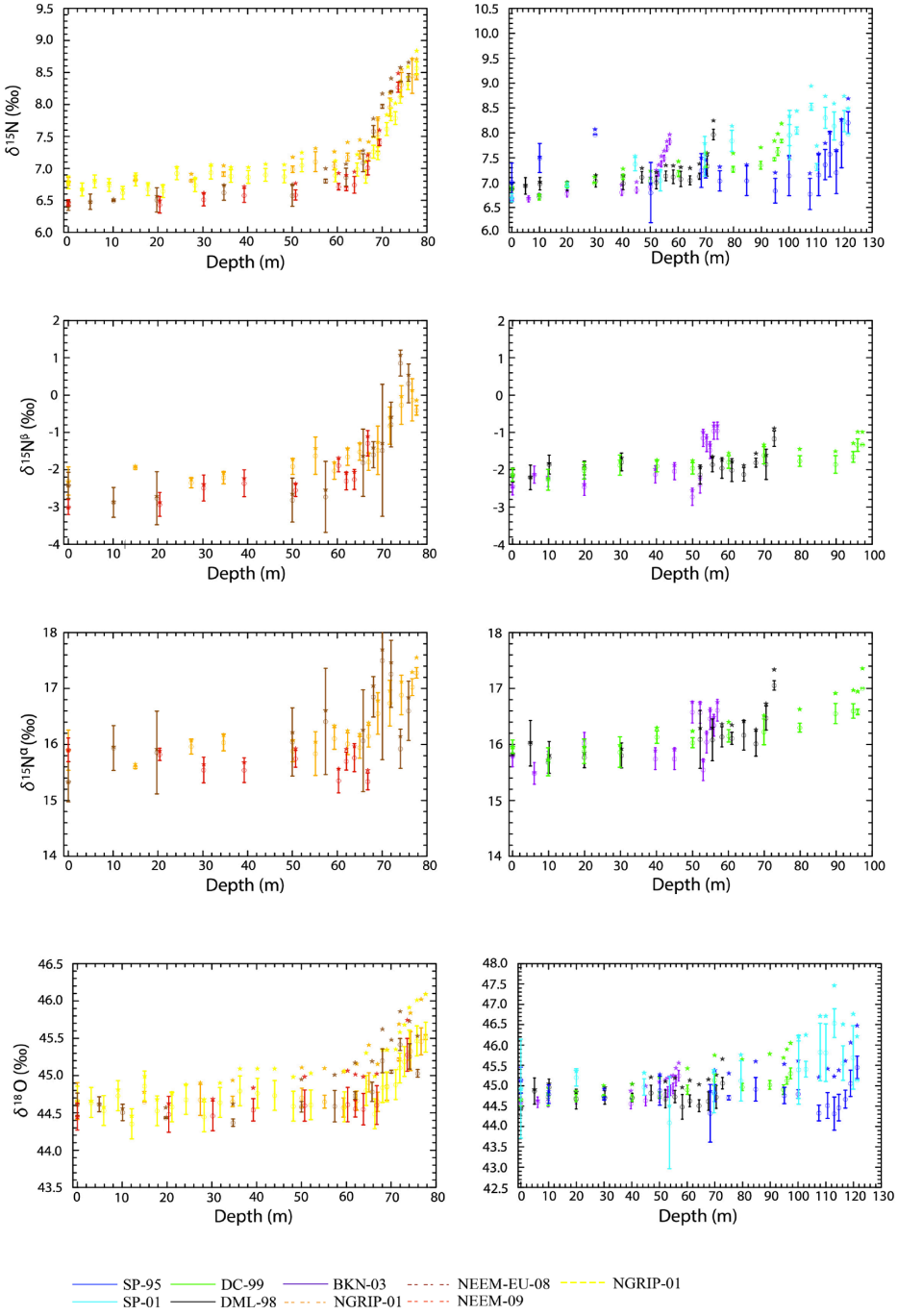

952

Atmos. Chem. Phys. Discuss., doi:10.5194/acp-2016-487, 2016
Manuscript under review for journal Atmos. Chem. Phys.
Published: 21 June 2016

Atmospheric Chemistry and Physics Discussions

Figure A1: Effect of firn fractionation on N_2O isotopic composition in firn. Original measurements are plotted as stars, data corrected for firn fractionation are plotted as circles with error bars. The right hand side shows Southern hemisphere sites, orange: NGRIP-01 (Bernard et al, 2006), yellow: NGRIP-01 (Ishijima et al, 2007), brown: NEEM-EU-08, red NEEM-09 and the left hand side shows Northern hemisphere sites, purple: BKN-03, black DML-98, green DC-99, blue SP-95 and light blue SP-01

Atmos. Chem. Phys. Discuss., doi:10.5194/acp-2016-487, 2016
Manuscript under review for journal Atmos. Chem. Phys.
Published: 21 June 2016

Atmospheric Chemistry and Physics Discussions

Appendix B: Data processing

In this study isotope deltas (δ) are used to denote the relative $^{15}N/^{14}N$ and $^{18}O/^{16}O$ ratio difference of N_2O in firn air with respect to a standard reference,

$$\delta^{15}N = \frac{R_{sample}}{R_{standard}} - 1 \quad (1)$$

where R represents the $^{15}N/^{14}N$ or $^{18}O/^{16}O$ abundance ratio of a standard or a sample. $\delta^{15}N$ values are reported relative to ^{15}R of atmospheric N_2, $\delta^{18}O$ values relative to ^{18}R of Vienna Mean Standard Ocean Water (VSMOW). The $^{15}N/^{14}N$, $^{18}O/^{16}O$ and position dependent $^{15}N/^{14}N$ isotope ratios were derived from measurement of the *m/z* 45 / *m/z* 44, *m/z* 46 / *m/z* 44 and *m/z* 31 / *m/z* 30 ion current ratios according to Kaiser et al., (2008), assuming a constant ^{17}O excess of 0.9 ‰.

There is a disagreement between reported trends of the position dependent $\delta^{15}N^{av}$ values reported in the literature from firn air on the one hand and archived air samples on the other hand (Park et al., 2012; Ishijima et al., 2007; Bernard et al., 2006; Röckmann and Levin, 2005; Röckmann et al., 2003; Sowers et al., 2002). In principle the temporal trend measured directly on archived air samples should be fully consistent with top firn air samples of the various data sets, which were collected over a decade or more, since the air in the diffusive zone is not very old. However, this is not the case. Using the high-precision determination of the temporal trend of the N_2O isotope signatures on archived air samples from Röckmann and Levin (2005) as reported in section 2.4 we rescale the different firn profiles to match this trend in the diffusive zone by interpolating the measurements from the diffusive zone of all sites to DC-99 (δ_{INT}). By using the firn model – assigned mean age of each sample, The maximum age difference from diffusive zone to surface corresponds to $\Delta age = \Delta_{DC\ t\text{-}t_0} = 10$ a. Below you can find the equations used:

$$\delta_{INT} = \delta_{t\text{-}t_0} - \delta_{DC\ t\text{-}t_0} + m\,(\Delta_{t\text{-}t_0} - \Delta_{DC\ t\text{-}t_0}) \quad (2)$$

$$\delta_{Final} = \delta_{meas} - (\delta_{exp} - \delta_{INT}) \quad (3)$$

Where m is the slope connecting the two points we want to interpolate. The applied scaling (δ_{Final}) is given in the Table B1 below. To bring the data to the most recent international scale, NOAA-2006A, we used an equation extracted from a correlation between a scale ratio of NOAA-2006A to CSIRO versus the mole fraction of N_2O. The correlation showed higher

Atmos. Chem. Phys. Discuss., doi:10.5194/acp-2016-487, 2016
Manuscript under review for journal Atmos. Chem. Phys.
Published: 21 June 2016

Atmospheric Chemistry and Physics Discussions

scale ratio for low fraction values and lower scale ratio for higher mole fraction values. The equation extracted is given below:

$$y(\text{NOAA-2006}) = -1.535 \times 10^{-4}\, y^2(\text{CSIRO}) + 1.045\, y(\text{CSIRO}) \qquad (4)$$

Atmos. Chem. Phys. Discuss., doi:10.5194/acp-2016-487, 2016
Manuscript under review for journal Atmos. Chem. Phys.
Published: 21 June 2016

Atmospheric Chemistry and Physics Discussions

Table B1. Implemented scaling for N_2O mole fraction and isotopic composition. The re-scaled average was extracted from the diffusivity zone for each site, which corresponds to the top 50 m. The expected trends are averaged values from CSIRO (http://www.csiro.au/greenhouse-gases) for the last 30 years for the mole fraction and measured trends from Röckmann and Levin (2005) for the isotopic composition. The rather large corrections to the isotope data from the SP-01 and SP-95 drillings are likely due to inter-laboratory scale differences.

Site	$y(N_2O)$(nmol mol^{-1})		
	Re-scaled average	**Expected trend change**	**Correction**
DML-98	0.09±0.29	-0.80±0.06	-0.89±0.32
NGRIP-01(Bernard)	3.39±0.54	1.60±0.06	-1.79±0.54
NGRIP-01 (Ishijima)	4.12±0.32	1.60±0.06	-2.52±0.32
BKN-03	3.47±0.22	3.20±0.06	-0.27±0.23
NEEM-EU-08	3.57±1.81	7.20±0.06	3.63±1.81
NEEM-09	8.84±1.82	8.00±0.06	-0.84±1.82

Site	$\delta^{15}N$ (‰)		
	Re-scale average	**Expected trend change**	**Correction**
SP-95	1.43±0.56	0.16±0.00	-1.27±0.56
DML-98	-0.18±0.12	0.04±0.00	0.22±0.12
SP-01	0.22±0.22	-0.08±0.00	-0.30±0.22
NGRIP -01(Bernard)	-0.18±0.07	-0.08±0.00	0.10±0.07
NGRIP -01 (Ishijima)	0.17±0.13	-0.08±0.00	-0.25±0.13
BKN-03	-0.17±0.12	-0.16±0.00	0.01±0.12
NEEM-EU-08	-0.63±0.15	-0.36±0.00	0.27±0.15
NEEM-09	-0.43±0.05	-0.40±0.00	-0.03±0.05

Atmos. Chem. Phys. Discuss., doi:10.5194/acp-2016-487, 2016
Manuscript under review for journal Atmos. Chem. Phys.
Published: 21 June 2016

Atmospheric Chemistry and Physics Discussions

Site	$\delta^{18}O$ (‰)		
	Re-scale average	Expected trend change	Correction
SP-95	-0.88±0.27	0.08±0.00	0.96±0.27
DML-98	0.26±0.15	0.02±0.00	-0.24±0.15
SP -01	0.74±0.62	-0.04±0.00	-0.78±0.62
NGRIP-01 (Bernard)	-0.08±0.05	-0.04±0.00	0.04±0.05
NGRIP-01 (Ishijima)	-0.17±0.12	-0.04±0.00	0.13±0.12
BKN-03	0.02±0.06	-0.08±0.00	-0.10±0.06
NEEM-EU-08	-0.21±0.15	-0.19±0.00	0.02±0.15
NEEM-09	0.28±0.04	-0.21±0.00	-0.49±0.04

Site	$\delta^{15}N^{\beta}$ (‰)		
	Re-scale average	Expected trend change	Correction
DML-98	-0.41±0.20	0.06±0.02	0.47±0.20
NGRIP-01 (Bernard)	-0.10±0.25	-0.13±0.02	-0.02±0.25
BKN-03	-0.53±0.30	-0.26±0.02	0.27±0.30
NEEM-EU-08	-0.33±0.27	-0.58±0.02	-0.25±0.27
NEEM-09	-0.14±0.17	-0.64±0.02	-0.50±0.17

Site	$\delta^{15}N^{\alpha}$ (‰)		
	Re-scale average	Expected trend change	Correction
DML-98	0.09±0.11	0.01±0.02	-0.08±0.11
NGRIP-01 (Bernard)	-0.26±0.19	-0.03±0.02	0.23±0.19
BKN-03	0.19±0.32	-0.06±0.02	-0.25±0.32
NEEM-EU-08	-0.61±0.35	-0.13±0.02	0.48±0.35
NEEM-09	-0.72±0.16	-0.14±0.02	0.58±0.16

Atmos. Chem. Phys. Discuss., doi:10.5194/acp-2016-487, 2016
Manuscript under review for journal Atmos. Chem. Phys.
Published: 21 June 2016

Atmospheric Chemistry and Physics Discussions

Appendix C: Atmospheric reconstruction re-scaled to NEEM-09 and without data re-scaling

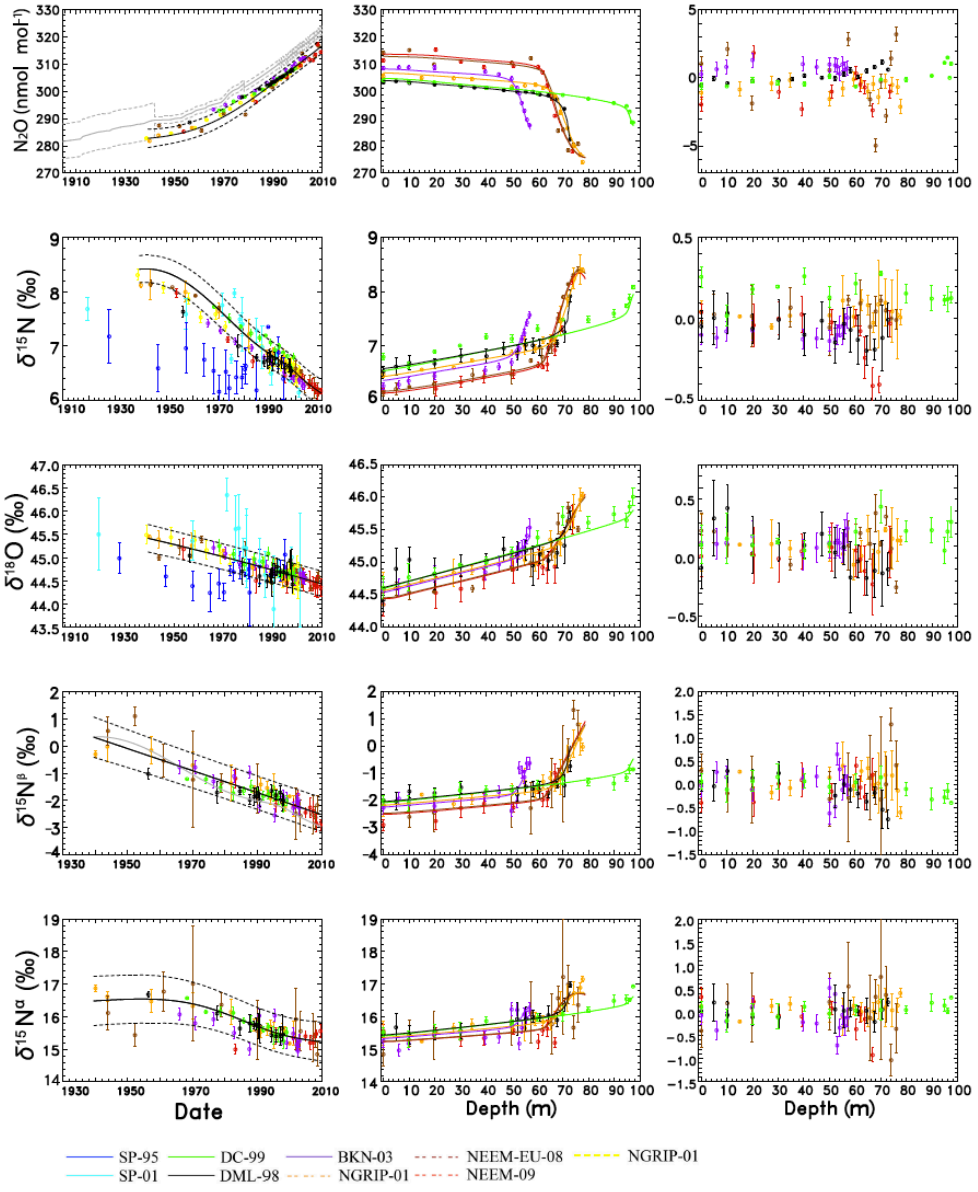

Figure C1. Results of the firn data evaluation (similar to Figure 2) using the data without re-scaling as indicated in the text, Orange: NGRIP-01 (Bernard et al, 2006), Yellow: NGRIP-01

Atmos. Chem. Phys. Discuss., doi:10.5194/acp-2016-487, 2016
Manuscript under review for journal Atmos. Chem. Phys.
Published: 21 June 2016

1024 (Ishijima et al, 2007), Brown: NEEM-EU-08, Red: NEEM-09, Purple: BKN-03, Black: DML-
1025 98, Green: DC-99, Blue: SP-95 and Light Blue: SP-01.

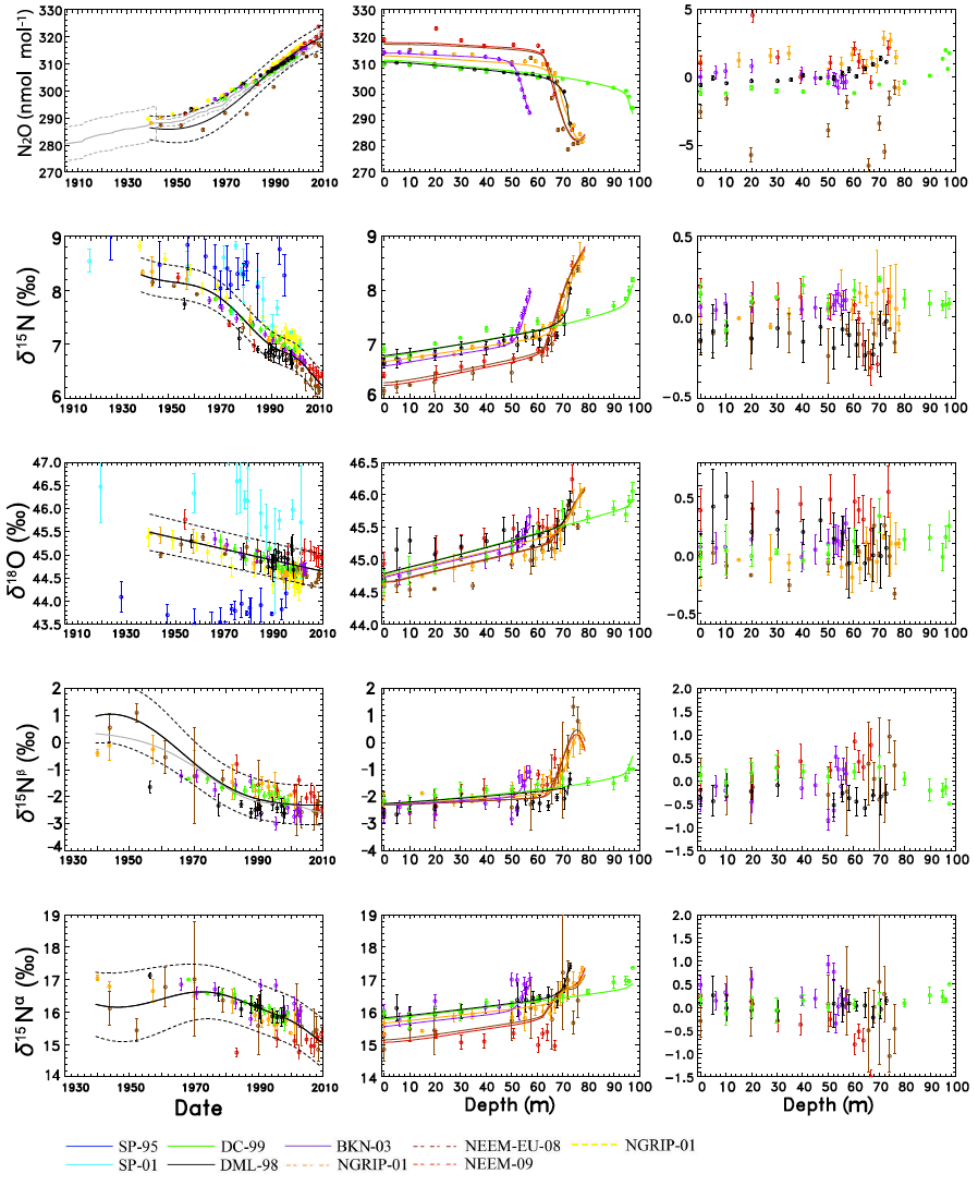

1026

1027 Figure C2. Results of the firn data evaluation (similar to Figure 2) using the data re-scaled to
1028 the NEEM-09 site. Colours as in Fig. C1.

1029

Atmos. Chem. Phys. Discuss., doi:10.5194/acp-2016-487, 2016
Manuscript under review for journal Atmos. Chem. Phys.
Published: 21 June 2016

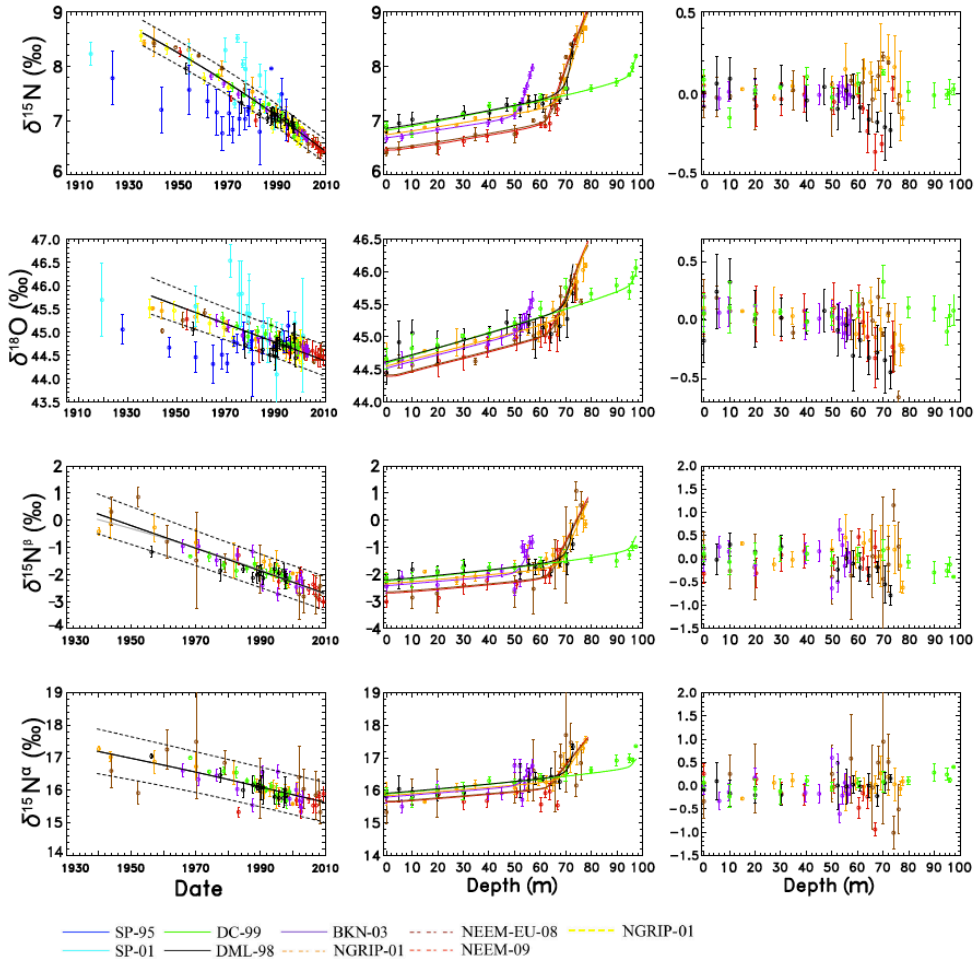

Figure C3. Sensitivity test for the regularization term. Reconstructed atmospheric scenarios (left), corresponding fit of the firn data (centre) and model data discrepancies (right). The best reconstructed scenarios are shown as the black continuous lines, with model derived uncertainties (2σ) in dashed lines. Colours as in Fig. C1.

Atmos. Chem. Phys. Discuss., doi:10.5194/acp-2016-487, 2016
Manuscript under review for journal Atmos. Chem. Phys.
Published: 21 June 2016

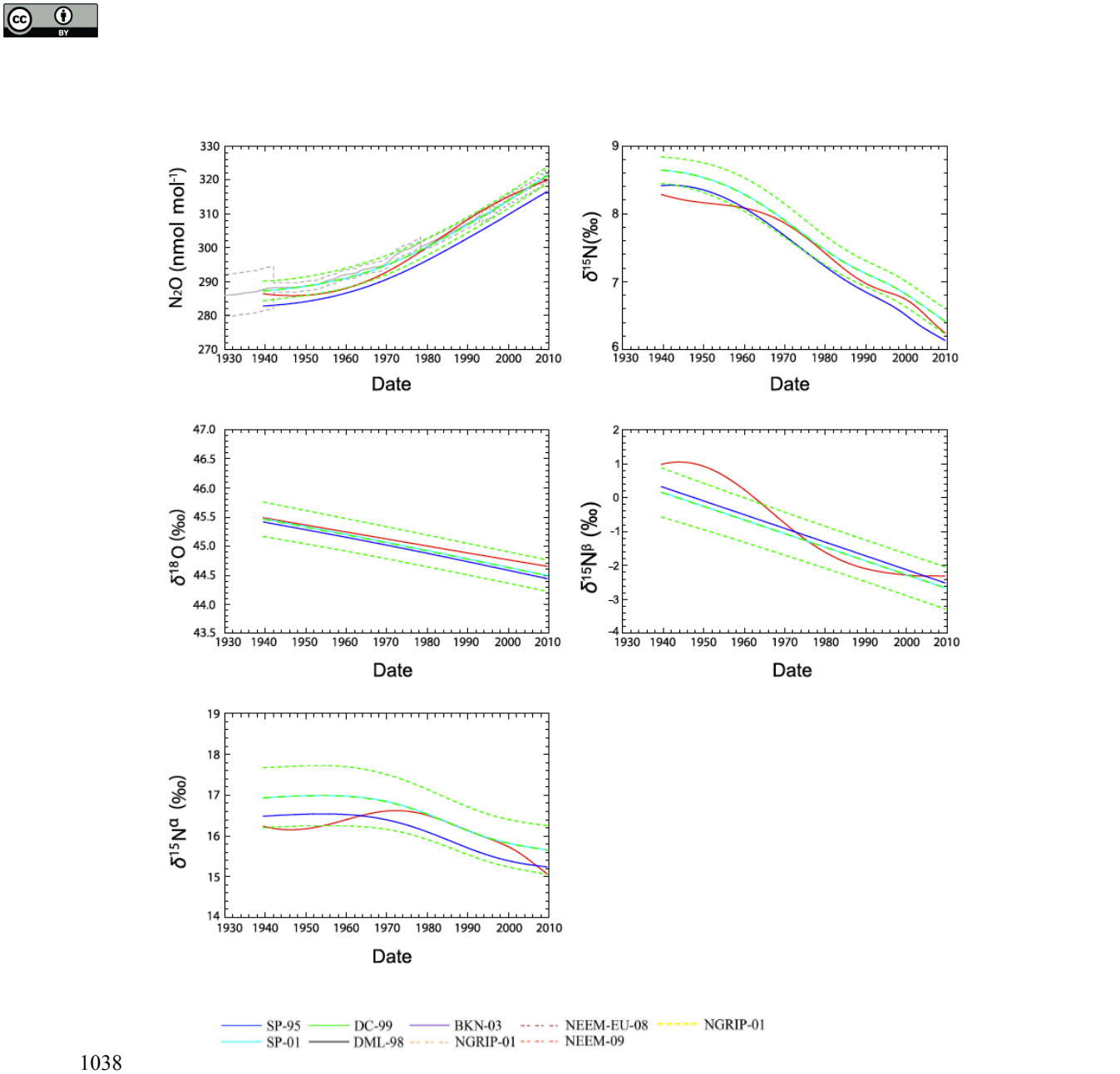

Figure C4. Comparison of the atmospheric reconstructions between different re-scaling methods. Solid and dashed green lines are the scenarios from data re-scaled to DC-99 used in this study. Solid red lines are the best-case scenario for the non re-scaled data and solid blue lines are the best-case scenarios from the data re-scaled to NEEM-09. The latter data series is shifted because of a calibration offset. When this is corrected for the data superimposes the green lines as expected.

Atmos. Chem. Phys. Discuss., doi:10.5194/acp-2016-487, 2016
Manuscript under review for journal Atmos. Chem. Phys.
Published: 21 June 2016

Atmospheric Chemistry and Physics Discussions

Appendix D: Sensitivity of the reconstructed N_2O emissions and isotopic signatures on N_2O lifetime.

For the default calculations with the mass balance model a constant lifetime for N_2O was used. A recent study from Prather et al. (2015), though, highlighted that top-down model calculations are sensitive to changes in the N_2O lifetime. To quantify the effect on our results we performed a sensitivity test where we linearly changed the N_2O lifetime from pre-industrial to modern times from 123 a in 1700 to 119 a in 2008. The results are shown in Figures D1 and D2 below.

In Figure D1 the N_2O atmospheric budget is re-calculated and compared with the results when the constant lifetime of 123^{+29}_{-19} a is used. In year 1940 the N_2O emissions are (12.3±2.7) Tg a^{-1} N and (17.0±1.7) Tg a^{-1} N in year 2008 with a total increase of (4.7±1.7) Tg a^{-1} N. When keeping the lifetime constant, the results for the same years are (11.9±1.7) Tg a^{-1} N and (16.4±1.7) Tg a^{-1} N with a total increase of (4.5±1.7) Tg a^{-1} N. This shows that there is a sensitivity on the choice of lifetime for our mass balance model on the N_2O atmospheric budget as was indicated by Prather et al. (2015).

The N_2O source isotopic signature shows no significant change with the choice of lifetime giving similar average source values for all source signatures as for when using a constant lifetime of 123^{+29}_{-19} a.

On the other hand, the N_2O average anthropogenic source signature displays a sensitivity in the choice of lifetime returning values (−15.9±2.6) ‰, (28.5±2.6) ‰, (−7.2±1.7) ‰ and (−22.8±8.4) ‰ for $\delta^{15}N^{av}$, $\delta^{18}O$, $\delta^{15}N^{\alpha}$ and $\delta^{15}N^{\beta}$ respectively. This agrees within combined errors with the total average values of (−18.2±2.6) ‰, (27.2±2.6) ‰, (−8.1±1.7) ‰ and (−26.1±8.4) ‰ for $\delta^{15}N^{av}$, $\delta^{18}O$, $\delta^{15}N^{\alpha}$ and $\delta^{15}N^{\beta}$ respectively when a constant 123^{+29}_{-19} a lifetime is used. On average, the N_2O anthropogenic signature results can differ by 10 % when a different lifetime is chosen, which is equivalent to a (2.0±1.0) ‰ difference in the final anthropogenic values.

Atmos. Chem. Phys. Discuss., doi:10.5194/acp-2016-487, 2016
Manuscript under review for journal Atmos. Chem. Phys.
Published: 21 June 2016

Atmospheric Chemistry and Physics Discussions

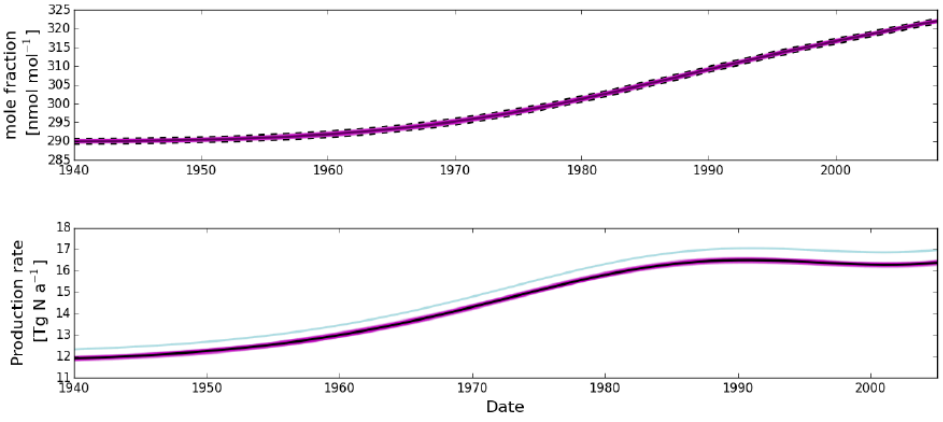

Figure D1: Top panel. N_2O mole fraction history from the multisite reconstruction (solid black line with uncertainty envelopes as dashed black lines) and the scenarios within the uncertainty envelopes that were used in the mass balance model (magenta lines) to evaluate the uncertainties of the atmospheric modelling results.

Bottom panel. N_2O production rate as calculated from the mass balance model assuming a change in the lifetime from 123 a in 1700 to 119 a in 2008 (relative change similar to Prather et al., 2015) in light blue. The solid black line represents the result for the best fit reconstruction while magenta lines represent the results for the individual scenarios from the top panel (lifetime kept constant at 123^{+29}_{-19} a) as used in the main paper.

Atmos. Chem. Phys. Discuss., doi:10.5194/acp-2016-487, 2016
Manuscript under review for journal Atmos. Chem. Phys.
Published: 21 June 2016

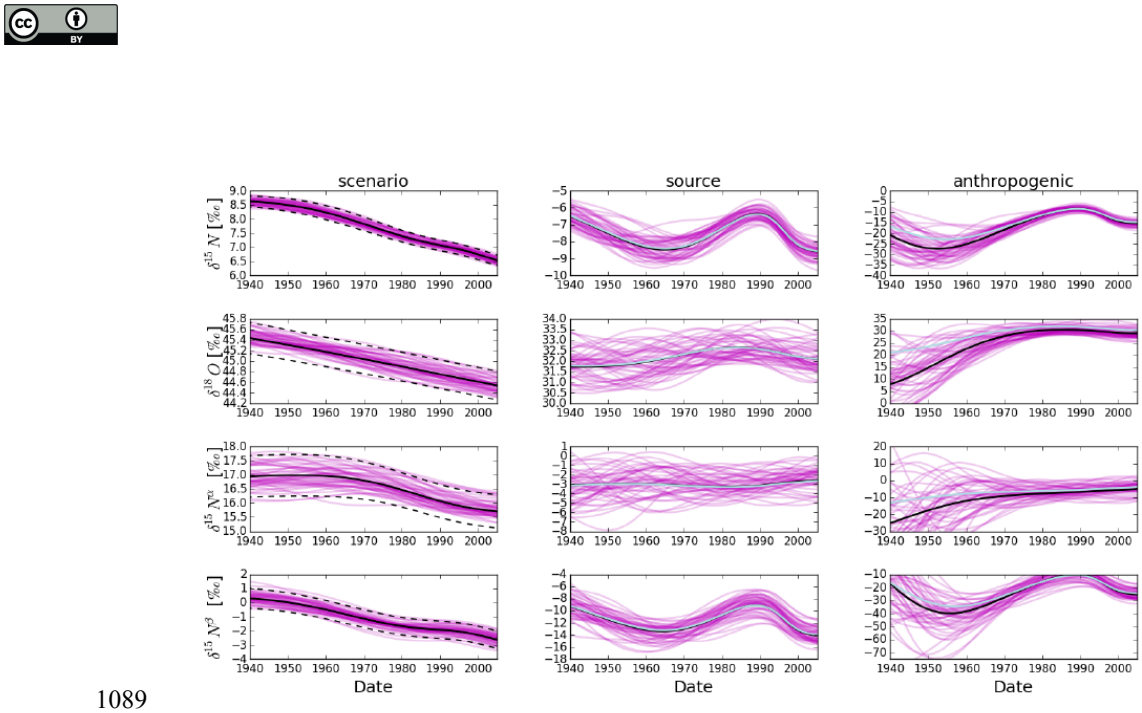

Figure D2: Left panels: Historic evolution of $\delta^{15}N$, $\delta^{18}O$, $\delta^{15}N^{\alpha}$ and $\delta^{15}N^{\beta}$ in N_2O as derived from the firn air reconstruction. The solid black line represents the best-fit scenario while the dashed ones represent the respective uncertainties as determined by the reconstruction method. Magenta lines represent the emissions that are required to produce the magenta N_2O histories in the left panels. Middle and right panels: Isotope signatures of the total emitted N_2O and anthropogenic source respectively assuming a change in the lifetime from 123 a in 1700 to 119 a in 2008 (relative change similar to Prather et al., 2015) in light blue. The solid black line represents the result for the best fit reconstruction while magenta lines represent the results for the individual scenarios from the top panel (lifetime kept constant at 123^{+29}_{-19} a) as used in the main paper.